2015

Magnetic Resonance Elastography of the Brain Using an Ergonomic Driver: Assessment of Scan-Rescan Reproducibility

Hatim Chafi
Louisiana State University and Agricultural and Mechanical College, hchafi1@lsu.edu

MAGNETIC RESONANCE ELASTOGRAPHY OF THE BRAIN USING AN ERGONOMIC DRIVER: ASSESSMENT OF SCAN-RESCAN REPRODUCIBILITY

A Thesis

Submitted to the Graduate Faculty of the
Louisiana State University and
Agricultural and Mechanical College
in partial fulfillment of the
requirement for degree of
Master of Science

in

The Department of Physics and Astronomy

by
Hatim Chafi
B.S., University of Pittsburgh, 2012
August 2015

ACKNOWLEDGMENTS

First, I thank my thesis committee for their assistance. I offer my sincere appreciation for the learning opportunities provided by my committee. I thank Drs. Lee and Dugas for agreeing to serve on my thesis committee. I thank my Thesis advisor Dr. Jia who has always been there for me, supporting me every step of the way. I will be forever grateful for his patience and guidance. I also thank Dr. Carmichael for allowing me to use the various resources at Pennington Biomedical Research Center imaging center. I cannot express enough thanks to Kori Murray for her invaluable help in recruiting and scheduling volunteers for this project. I also thank Dr. Matthews for always making me feel welcomed in his office, and answering all my technical questions.

My completion of this project could not have been accomplished without the support of Ryan Schurr. His friendship was invaluable to me. I thank fiancé Janet for her unconditional love and support. I acknowledge my brother Hassan whose work ethic has always been an inspiration to me.

Most importantly, I thank my parents. In particular, I thank my mother Linda for believing in me. I dedicate this thesis to her. I thank my father Abdellatif for all the entertaining and intellectually stimulating telephone conversations that made me feel like I never left home.

TABLE OF CONTENTS

LIST OF TABLES

LIST OF FIGURES

ABSTRACT

Magnetic resonance elastography (MRE) allows the visualization of displacement patterns from induced harmonic mechanical waves propagating in tissue. Strain and mechanical properties can be computed from these displacement patterns. Mechanical properties of tissue are affected by various disease processes. MRE has shown brain tumor to differ in stiffness in comparison to normal tissue. MRE is currently being offered as an upgrade on most conventional MRI scanners. However, the actuator supplied by vendors is a drum driver designed primarily for hepatic MRE scan. The goals of the project was to design and build an ergonomic flexible driver for use in MRE of the brain, to assess the Scan-Rescan reproducibility of shear modulus measurements, and to investigate the relationship between shear modulus measurements and driver frequency.

An ergonomic flexible driver was constructed to induce mechanical waves in the brain. MRE of the brain was performed in 10 healthy volunteers. MRE data was collected at frequencies of 60 Hz, 50 Hz, and 40 Hz. After the scans were completed, the subjects were removed from the table, and then repositioned and rescanned using the same process. All subjects were scanned and rescanned within an hour. The within-subject coefficient of variance (CV) and inter-subject CV were calculated for shear modulus measurements of white matter, grey matter, and whole brain. A one-way analysis of variance (ANOVA) was applied to test for any difference between shear modulus measurements made at different frequencies.

The within-subject CVs of white matter, grey matter, and whole brain shear modulus measurements for all frequencies ranged from 3.7-4.1%, 4.7-6.0%, and 1.8-3.5% respectively. A significant statistical difference was found between measurements made at different frequencies. This study demonstrated the ability to make in vivo shear modulus measurements of brain tissue.

MRE was shown to be able to differentiate white matter from grey matter using the shear modulus. Measured white and grey matter shear modulus values were within the range of values reported in literature. A dependence of shear modulus measurements on frequency was observed; Standardization of MRE imaging parameters is recommended to facilitate the interpretation of brain MRE results.

CHAPTER 1: INTRODUCTION

1.1 MAGNETIC RESONANCE ELASTOGRAPHY

Palpation is a clinical tool that allows the assessment of viscoelastic properties of tissue which are affected by various disease processes (Manduca, Oliphant et al. 2001). The presence of a hard mass in the breast, thyroid, or prostate indicates of the likelihood of malignancy. CT, MRI, and ultrasound do not directly provide information regarding the elastic properties of human tissue. The property assessed by palpation is the elastic modulus (Mariappan, Glaser et al. 2010). The shear modulus of tissues varies over five orders of magnitude, while the tissue properties assessed by CT, MRI, and ultrasound vary over a much smaller range (Figure 1.1) (Mariappan, Glaser et al. 2010).

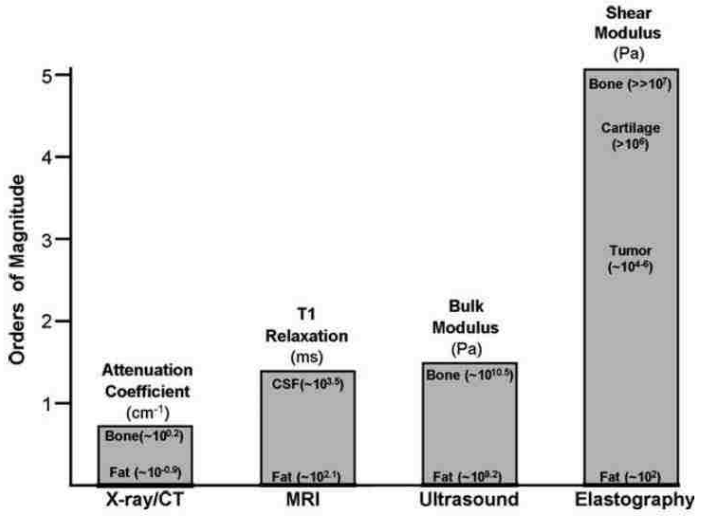

Figure 1.1: Summary of the contrast mechanisms utilized by them. The shear modulus has the largest variation, over five orders of magnitude among various normal and pathologic tissues (Mariappan et al., 2010). Adapted from Mariappan 2010

Magnetic resonance elastography (MRE) allows the spatial mapping of displacement patterns resulting from harmonic mechanical waves with amplitudes of 1 μm (Muthupillai, Lomas et al. 1995). Strain and other mechanical properties can be computed from these

displacement patterns. This allows the noninvasive inferrance of mechanical properties of a wide range of solid materials. The technology is becoming available as an upgrade on conventional MRI scanners (Mariappan, Glaser et al. 2010).

MRE is performed by generating shear waves with the use of an external driver. The driver is a drum-like paddle which is connected to an enclosed speaker cone outside the MRI unit by a long connecting tube. The propagating waves are imaged inside the body using a phase-contrast technique with the help of motion encoding gradient pairs (Muthupillai, Lomas et al. 1995). The resulting data are processed to generate quantitative images displaying stiffness maps, also known as elastograms.

1.2 PHYSICS OF MRE

MRE uses an external driver to induce harmonic motion at a frequency range of 40-500Hz. The electrical signal that powers the external drivers is triggered by and synchronized to the MR pulse sequence. The most widely used method for generating waves in tissue, is to enclose the area around a speaker cone or its equivalent, and use a long connecting tube to pneumatically conduct harmonic pressure variations of air into the scanner room; the tube terminates at a passive drum-like driver kept in contact with the tissue (Figure 1.2). The Lorentz force is the process by which vibrations are generated in these acoustic speaker systems (Mariappan, Glaser et al. 2010). Due to having their own permanent magnets, acoustic speaker systems must be placed outside the scanner room. Additional MR compatible components are needed to transfer the vibrations to the tissue. Generally, an anti-kink supply tube connected to the passive driver is used for that purpose. The passive driver is designed to optimally generate shear waves in the organ of interest, such as the pancreas (Shi, Glaser et al. 2015) , liver (Yin, Talwalkar et al. 2007), and brain (Murphy, Huston et al. 2011). To prevent biological damage, the

vibrations are typically limited to levels deemed safe by regulatory entities, such as the European Union (Ehman, Rossman et al. 2008) .

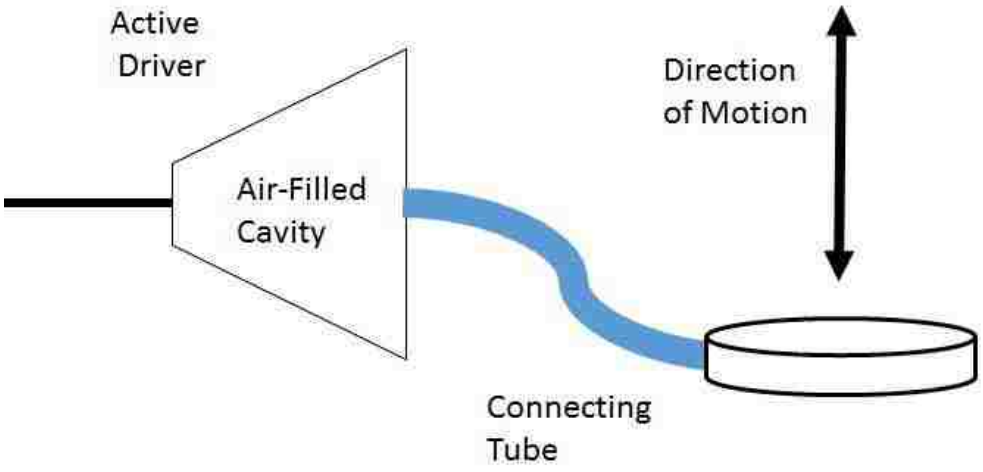

Figure 1.2: Schematic drawing of an enclosed speaker coupled to an MR compatible connecting tube and passive driver.

Perturbations in the compressional component of the displacement vector propagate as compressional waves with a speed:

$$C_c = \sqrt{\frac{\lambda+2\mu}{\rho}} \qquad [1]$$

where λ is Lamés elasticity constant, μ is the shear modulus, and ρ is the density of the material (Muller 2007). The shear modulus describes an object's tendency to shear, which is the deformation of shape at constant volume when acted upon by opposing forces. The perturbation in the shear component of the displacement vector propagates as shear waves with a speed:

$$C_s = \sqrt{\frac{\mu}{\rho}} \qquad [2]$$

Compressional and shear waves are called longitudinal waves and transverse waves, respectively. The displacement vector in a shear wave is perpendicular to the compressional displacement vector. Compressional waves and shear waves decouple in a homogeneous medium. Both waves create reflected and refracted waves of the other type at interfaces.

Muthupillai et al. developed MRE by modifying phase-contrast MRI (Muthupillai, Lomas et al. 1995). MRE data are collected by inducing continuous harmonic motion in tissue, applying a motion encoding gradient MEG at same frequency as of the passive driver, and performing conventional MR imaging. The phase contribution ϕ to the MR image due to the induced motion and the applied field gradient at a given position vector $\mathbf{u}$ and phase offset θ between the motion and the MEG is expressed as:

$$\phi(\mathbf{u}, \theta) = \frac{\gamma NT(\mathbf{G}\cdot\boldsymbol{\xi_0})}{2}\cos(\mathbf{k}\cdot\mathbf{u} + \theta) \quad [3]$$

where γ is the gyromagnetic ratio of the tissue protons ($\gamma/2\pi$ = 4257 Hz/G), N is the number of gradient pairs used to sensitize the motion, T is the period of the MEG, $\mathbf{G}$ is the amplitude of the MEG, $\boldsymbol{\xi_0}$ is the peak amplitude of the motion, θ is the phase offset between the harmonic motion and the MEG, and $\mathbf{k}$ is the wave number. The phase of harmonically vibrating tissue is directly proportional to its displacement. The MEG is applied after the RF excitation of the tissue but before the measurement of the induced signal. Motion occurring along any spatial dimension can be encoded into the phase of the MR image by manipulating the axes on which the MEGs are placed.

MRE is sensitive to repetitive displacement amplitudes of 100s of nm (the characteristic displacement for shear moduli of soft tissues). An MR image containing information about the propagating wave at a particular phase is called a wave image. Non-motion-related phase

information is removed by collecting two wave images with opposite polarity of the MEG and calculating the phase-difference image. Acquiring multiple snapshots of the propagation of the wave is accomplished by varying the phase offset between the harmonic motion and the MEG. Typically, 4-8 temporal samples are spaced equally over a period of the wave motion, to show the wave propagation in MRE experiments and allow the processing of the data over time.

The complex value of the shear modulus can be obtained using an inversion method termed algebraic inversion of the differential equation (AIDE). The algorithm works by direct inversion of a differential equation of motion using local polynomial fits to the data (Oliphant, Manduca et al. 2001). Assuming local homogeneity, the shear modulus μ is related to displacement $\boldsymbol{u}$ by:

$$\mu\nabla^2\boldsymbol{u} + (\lambda + \mu)\nabla(\nabla \cdot \boldsymbol{u}) = -\rho\omega^2\boldsymbol{u} \quad [6]$$

where λ is a constant related to the longitudinal deformation of the material. λ is much larger than μ in soft tissue. Determining λ and μ is referred to as Full AIDE inversion. The accurate estimation of λ is challenging because the longitudinal wavelength in tissues is on the order of tens of meters. Assuming the displacements due to the longitudinal wave vary slowly, the $\lambda(\nabla \cdot \boldsymbol{u})$ term in equation [6] reduces to zero. The equation of motion reduces to:

$$[\nabla(\nabla \cdot \boldsymbol{u})\nabla^2\boldsymbol{u}]\mu = -\rho\omega^2\boldsymbol{u} \quad [7]$$

All three spatial components of the motion are required to obtain μ. Making the assumption that the material is incompressible makes the $\nabla \cdot \boldsymbol{u}$ term reduce to zero. The equation of motion then simplifies to:

$$\mu\nabla^2\boldsymbol{u} = -\rho\omega^2\boldsymbol{u} \quad [8]$$

The inversion of this simplified equation allows the estimation of the shear modulus from a single polarization of motion. This method is referred to as incompressible AIDE, or Helmholtz inversion.

1.3 CLINICAL APPLICATION OF MRE

MRE has been used clinically to assess hepatic fibrosis which increases liver stiffness (Yin, Talwalkar et al. 2007). Hepatic fibrosis is a reversible wound-healing response characterized by the accumulation of extracellular matrix following liver injury (Hernandez-Gea and Friedman 2011). If injury to the liver is sustained, chronic inflammation occurs, and liver tissue is progressively replaced by scar tissue. Fibrosis can lead to cirrhosis, the end consequence of progressive fibrosis. Chronic liver disease and cirrhosis is the 10^{th} leading cause of death in the United States (Kim, Brown et al. 2002). The gold standard for detecting hepatic fibrosis is percutaneous liver biopsy. However this technique causes discomfort to patients and, although rare, intraperitoneal hemorrhage can occur (Bravo, Sheth et al. 2001). MRE can non-invasively detect hepatic fibrosis with a 98% sensitivity and 99% specificity 98%. MRE can also discriminate between healthy volunteers and patients with moderate or severe fibrosis (Yin, Talwalkar et al. 2007). Cirrhosis can be a precursor to the development of hepatocellular carcinoma. In one study, the shear modulus measured by MRE for malignant liver tumor(10.1 kPa) was significantly greater than for benign tumors (2.7 kPa, $P < 0.001$) and for fibrotic liver (5.9 kPa, $P < 0.001$) (Venkatesh, Yin et al. 2008). This study showed the potential for assessing solid liver tumors with MRE.

1.4 MRE OF THE BRAIN

Obtaining information about brain tissue's mechanical properties may help to understand the mechanics of brain injury. Several studies have measured shear modulus in the brain in healthy volunteers. MRE has shown that brain tumors differ in stiffness compared to normal

brain tissue (Di Ieva, Grizzi et al. 2010). Shear modulus values for white and grey matter ranged from 2.7 kPa to 15.2 kPa, and 3.1-12.9 kPa, respectively. The data generally indicated that white matter was stiffer than grey matter (Table1.1). However, the variability of that data provided no definitive values for the absolute magnitudes of brain tissue stiffness in vivo.

In a study comparing stiffness to loss of brain volume, MRE was applied to 17 MS patients and 42 healthy volunteers. The results showed a decrease in stiffness of the brain parenchyma of MS patients with a highly significant change observed in female patients over male patients. Disease-related brain atrophy was apparent in women while no effect was observed in men (Streitberger, Paul et al. 2010) . MRE of the brain also showed reduced brain tissue stiffness in patients with Alzheimer's disease (Murphy, Huston et al. 2011).

Table 1.1: White and grey matter shear modulus values reported by various authors.

Study	μ White Matter [kPa]	μ Grey Matter [kPa]
Kruse et al. 2008	13.6	5.22
Green et al. 2008	2.7	3.1
McCraken et al. 2005	11.6	7.5
Uffmann et al. 2004	15.2	12.9

Measuring and monitoring mechanical properties of a tumors and the surrounding brain tissue may provide valuable information about the tumors progression and response to treatment.Six patients with confirmed solid brain tumors were evaluated by Xu et al (Xu, Lin et al. 2007). Of the six cases, four were meningiomas, one was a schwannoma, and one was a hemangiopericytoma. MRE images were evaluated by a radiologist to classify tumor elasticity as less than, similar to or greater than that of white matter. Subsequently, all six cases were evaluated intra-operatively by a single surgeon who was blinded to the MRE results. The elasticity of the tumors agreed with the surgeon's assessment for all cases. Figure 1.4 shows three cases of brain meningiomas. Transitional meningiomas had either a higher or lower elasticity compare to that of the white matter. Fibrous meningiomas had elasticity comparable to

that of white matter. Shwannoma and hemangiopericytoma had higher elasticity compared to that of white matter.

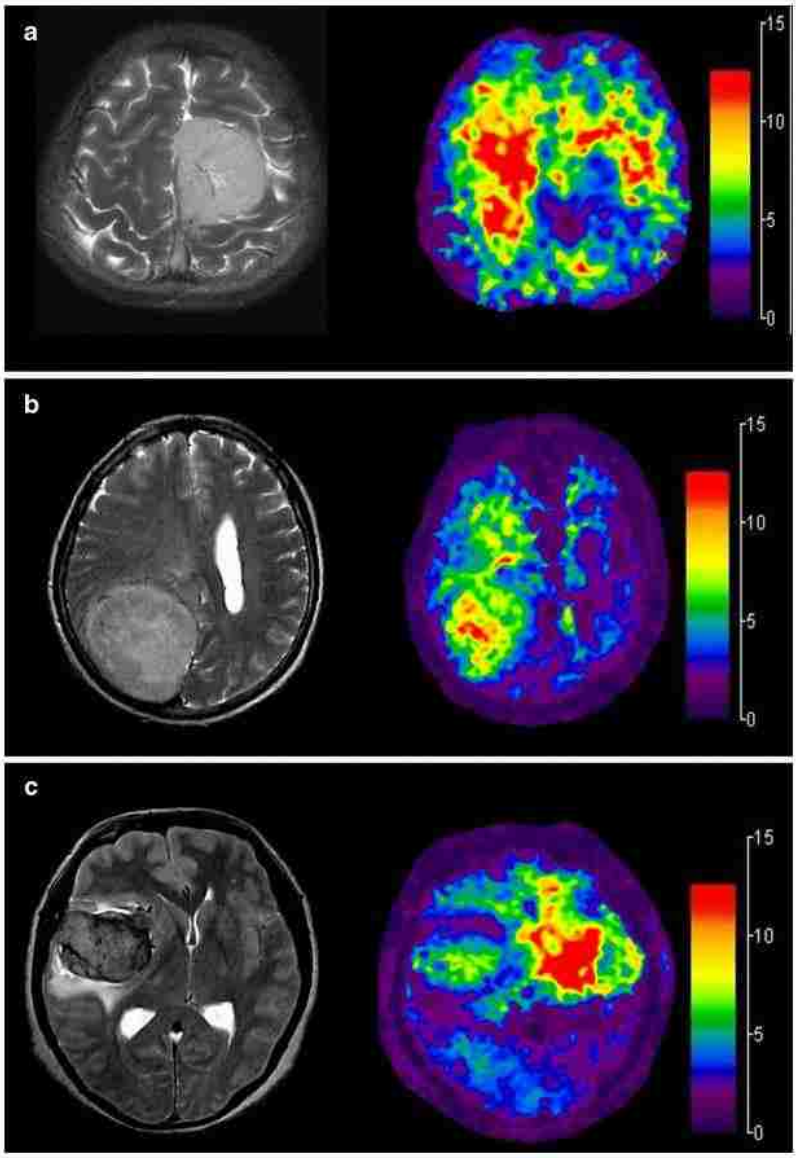

Figure 1.3: Three cases of brain meningiomas. On the left, T2-weighted images showing large brain menigiomas. On the right is shown the elastogram generated from MRE. (a) A transitional meningioma in the left parasagittal frontal lobe showed lower stiffness compared to that of white matter. (b) In another transitional meningioma case, located in the right parietal isointense to the cortex, showed higher stiffness compared to that of white matter. (c) A fibrous meningioma, with an isointense signal to the cortex, showed the elastic modulus was similar to that of white matter (Xu, Lin et al. 2007). Adapted from Xu 2007

1.5 MOTIVATION FOR RESEARCH

The goal of this project was to design and build an ergonomic flexible driver for use in MRE of the brain. MRE is a quantitative imaging technique that allows the noninvasive measurement of stiffness in regions of the body that aren't accessible through palpation. This Thesis summarizes the theory of MRE, and its current and potential applications. MRE can potentially be used to differentiate radiation induced necrosis from tumor recurrence. A human study was used to evaluate the performance of the ergonomic flexible driver when used for MRE of the brain.

1.6 HYPOTHESIS AND SPECIFIC AIMS

The hypothesis of this work was that white and grey matter shear modulus measurements made with MRE using a flexible, ergonomic driver will be reproducible with a within-subject coefficient of variation below 15% at a single frequency. There will be no statistically significant difference ($P < 0.05$) between shear modulus measurements made at driver frequencies of 60 Hz, 50 Hz, and 40 Hz.

To test the hypothesis, a passive drive was designed and fabricated for the application of brain imaging. Then two specific aims were completed.

Aim 1: Assessment of scan-rescan reproducibility. MRE of the brain was performed in 10 healthy volunteers on a 3T MRI scanner using a 2D echo planar imaging (EPI) MRE sequence. Shear waves were induced at frequencies of 60 Hz, 50 Hz, and 40 Hz, using an ergonomic flexible driver connected to a speaker system via a polyvinyl chloride tube. Each subject was repositioned and rescanned within one hour.

Aim 2: Compare shear modulus measurements between driver frequencies. Shear modulus measurements between driver frequencies were compared by performing an analysis of variance test.

CHAPTER 2: MATERIALS AND METHODS

2.1 ERGONOMIC FLEXIBLE DRIVER DESIGN AND CONSTRUCTION

2.1.1 PASSIVE DRIVER REQUIREMENTS

Several factors were considered when designing the passive driver. Passive drivers are kept in contact with the patient. Therefore, it was essential to use materials that are MRI compatible. The driver needed to occupy a minimal amount of volume inside an MRI head coil. Because the area of interest was the brain, an ergonomic design was sought, to avoid discomfort for the MRE scan subjects. A passive driver design that was activated pneumatically was chosen. The brain MRE driver had to ensure that the air being pumped into it distributed uniformly. An active driver placed outside of the MRI scanner provided the air flow to the passive driver. The MRI system used for this study provided a passive drum driver primarily designed for hepatic MRE scans. The hepatic driver is 19 cm in diameter and very rigid making it unsuitable for MRE brain scans (Figure 2.1).

Figure 2.1: The hepatic driver (Resoundant, Inc. Rochester, MN) provided with the MRI system.

The passive driver needed to be soft and compressible. A solid flexible structure was needed to ensure that the driver was inflated at initial static condition. The driver should not be compressed by weight of the subject's head before the active driver starts pumping air into it. The flexible structure should also allow air to flow efficiently.

2.1.2 PASSIVE DRIVER CONSTRUCTION

Figure 2.2 shows the flexible ergonomic driver that was created for this work. An adjustable air filter was chosen to act as the core of the solid flexible structure of the passive driver. The air filter (3M, St Paul, MN) was made from fiberglass and had a thickness of 2.5 cm. The air filter was cut to a circle of a diameter of 15.2 cm. A polyvinyl chloride PVC tube of an inside diameter of 1.3 cm was attached to the air filter. Two circular cutouts, made out of a supple PVC fabric (Gaiam. Louisville, CO), were stitched together to encase tightly the air filter and the PVC tube. The edges of the two cutouts were glued together to ensure that a minimal amount of air would leak during the scan. An MRI skin marker was glued on the center of the driver to assist alignment of the driver in the imaging area of interest.

2.1.3 ACTIVE DRIVER

The Resoundant active driver was placed outside the MRI room (Figure 2.3). The active driver was connected via a BNC cable and an Ethernet cable to the MRI scanner (GE MR750W 3.0T, GE Healthcare). This scanner has a 75 cm bore and operates at magnetic field strength of 3T. The signal generator in the active driver was triggered by and synchronized to the MRE pulse sequence. The active driver was connected by a 7.3 m PVC tube which connected to the passive driver inside the MRI suite.

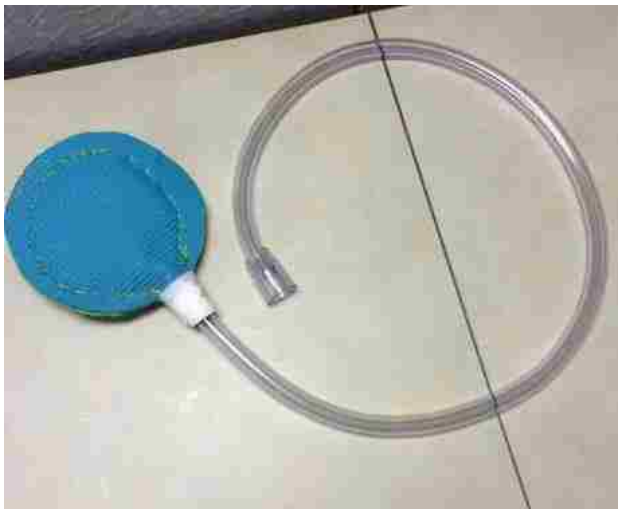

Figure 2.2: The ergonomic flexible driver designed for MRE brain scans. The flexible reducer was connected the passive driver's tube to the active driver located outside the scanner room.

Figure 2.3: The Resoundant active driver system located in the equipment room. The active driver pneumatically transmitted harmonic pressure variations to the passive driver kept in contact with the subject.

2.2 IMAGE ACQUISITION

2.2.1 SUBJECT POPULATION

This study was approved by the institutional review board at Pennington Biomedical Research Center. Brain MRE studies were performed in 10 healthy volunteers, 6 males and 4 females (mean age: 28 years, range: 24-38 years, mean weight: 77.2 kg, range: 48.7-94.4 kg). All subjects provided written informed consent. The inclusion criteria for the study were that subjects must be between the age of 18 and 50, with no metal fragments in the body, free of metallic tattoos, and weigh under 227 kg; females must be non-pregnant. Table 2.1 lists the subjects' age, sex, and weight.

Table 2.1: Subjects' age, sex, and weight

Subject #	Age [years]	Sex	Weight [kg]
1	26	F	48.7
2	26	F	85.5
3	24	M	77.6
4	31	M	71.5
5	26	M	64.3
6	26	M	94.4
7	38	M	93.7
8	26	F	61
9	28	F	78.5
10	25	M	79.6

2.2.2 IMAGING PROTOCOLS

Subjects were scanned head first in a supine position. The driver was placed directly behind the subject's head. Care was taken to make sure that the MR skin marker (Beekley Medical, Bristol, CT) was centered in the area of interest on a localizer scan. Axial T2-weighted images were acquired covering the whole brain using a spin echo SE sequence. A single slice was selected that encompassed the prefrontal lobe, temporal lobe, corpus callosum, and occipital lobe (Figure 2.4); the slice was centered on the passive driver. The parameters for the SE sequence are listed in Table 2.2. This slice was used to acquire eight magnitude images, and

eight phase images at 8 temporal phases using a 2D echo-planar imaging (EPI) MRE sequence. The active driver was synchronized with the EPI pulse sequence. The sequence was modified from a typical EPI sequence to include motion-encoding gradients. MRE sequence parameters are in listed in Table 2.2. MRE data was collected at frequencies of 60 Hz, 50 Hz, and 40 Hz. Driver amplitudes was fixed for all subjects and care was taken to make sure that shear wave propagation was visible on the phase images. The motion encoding frequency was set to match the driver frequency. The motion encoding gradient was set in the through plane (Z) direction. After the scans were completed, the subjects exited the table, they then repositioned on the table and rescanned using the same process. All subjects were scanned and rescanned within one hour.

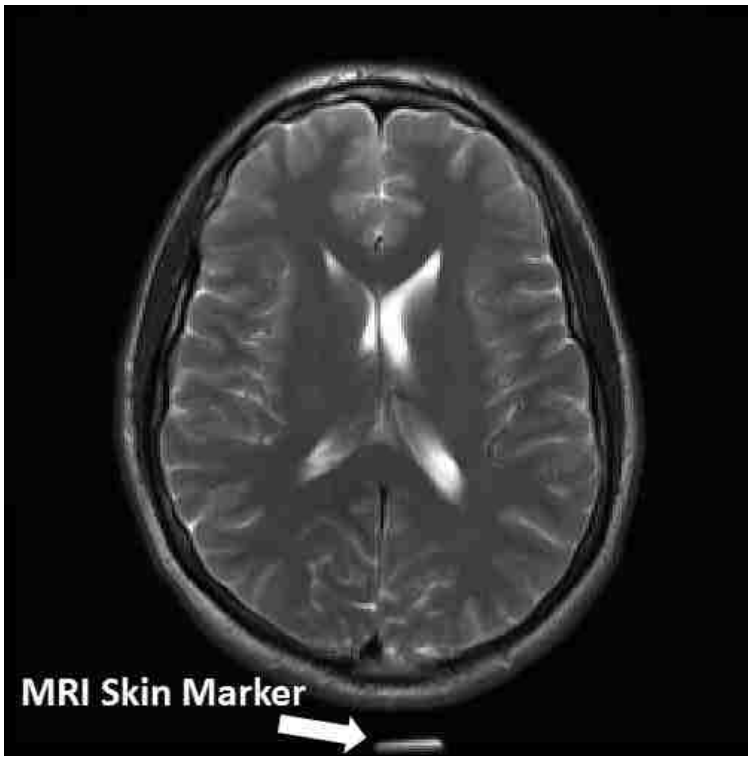

Figure 2.4: T2 weighted image showing a transverse slice of brain and the MRI skin marker. . The skin marker is located on the center of the passive driver. The slice of interest is located at the center of the passive driver to ensure adequate wave propagation.

Table 2.2: Imaging sequence parameters used for SE and MRE acquisitions (N/A= not applicable).

Sequence Type	T2-Weighted SE	2D MRE EPI
TR	3000 ms	1000 ms
TE	94.4 ms	62-84ms
Flip Angle	142	90º
Acquisition Matrix	256 × 256	64 × 64
Field of view	24 cm	24 cm
Slice Thickness	10 mm	10 mm
Temporal Phases	N/A	8
Driver/ MEG Frequencies	N/A	60, 50, 40 Hz

2.3 IMAGE ANALYSIS

2.3.1 WHITE AND GREY MATTER SHEAR MODULUS CALCULATIONS

MRE data was reconstructed using GE MR Touch (DV23.1, GE Healthcare) processing software. This post-processing software performed Helmholtz inversion on the MRE data. The algorithm assumed that the material was incompressible. The software unwrapped the phase images by using a quality map to process high-quality pixels first and low-quality pixels last. The quality map defined the quality of each phase value by using the variance of phase derivatives, maximum phase gradients, the magnitude image, and the pseudocorrelation. Phase images were converted into wave images which display the displacement of the tissue in the direction perpendicular to the slice. Inversion was subsequently applied to the wave data, and a grey scale elastogram was generated (Figure 2.5).

Once the grey scale elastograms were created, ImageJ processing software (ImageJ 1.48v, National Institutes of Health) was used to draw ROIs on the T2-weighted images in the white matter, the grey matter, and the whole brain (Figure 2.6A). Two ROIs encompassed white matter. The same was done for grey matter measurements. The ROI of the whole brain was drawn as a single composite ROI encompassing the whole brain. The ROIs were placed in areas where adequate wave propagation was clearly visible (Figure 2.6B). The ROIs were copied and

pasted onto the elastogram, and measurements were made and averaged for white and grey matter. An elliptical mask was applied to the elastograms to exclude noise. The grey scale elastograms were saved as text images and imported into MATLAB version R2013a (Natick, Massachusetts) to apply a jet color map and add a color bar in units of kPa (Figure 2.6C) for the purpose of display. The shear modulus (μ) was measured in white matter, grey matter, and the whole brain from both the scan and rescan data. At each of the three frequencies, the mean and standard deviation of μ for white matter, grey matter, and whole brain were calculated for all patients using the scan and rescan data..

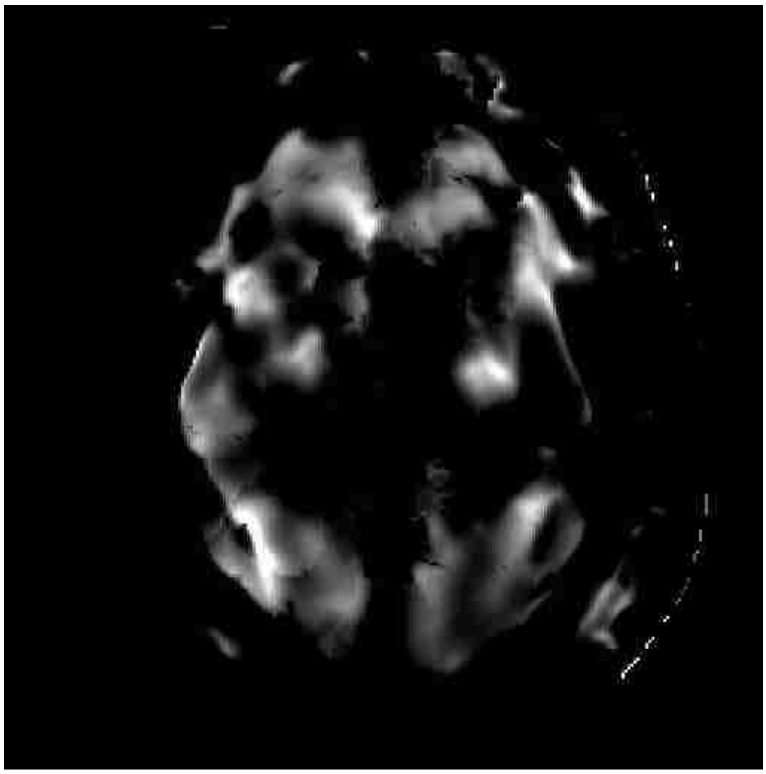

Figure 2.5: Grey scale elastogram generated by the GE MR Touch (DV23.1) processing software.

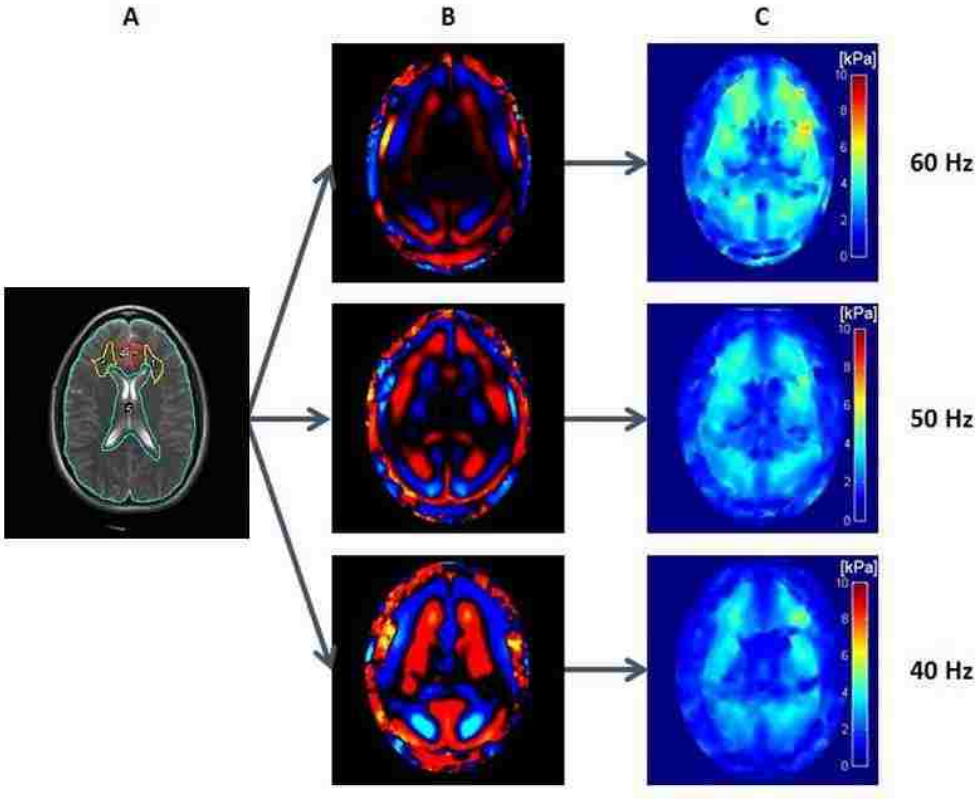

Figure 2.6: (A) A single T2-weighted image was used as anatomical reference for the MRE scans at all three driver frequencies. The yellow, red, and blue ROIs encompass white, grey, and whole brain, respectively. (B) Wave images showed adequate shear wave propagation in the ROIs. (C) Elastograms were reconstructed by the Helmholtz inversion algorithm.

2.3.2 WHITE AND GREY MATTER SHEAR MODULUS COMPARISON

The Wilcoxon signed-rank test was chosen to test for a significant statistical difference between white and grey matter shear modulus measurements. The Wilcoxon signed-rank test is an alternative to the two sample Student *t*-test, used if the distribution of differences between the pairs cannot be assumed to be normally distributed. This test assumes that data were paired and came from the same population, and that each pair was chosen randomly and independently. The test was applied to compare white and grey matter shear modulus measurement at all three frequencies.

2.4 AIM 1, ASSESSMENT OF SCAN-RESCAN REPRODUCIBILITY

2.4.1 SHEAR MODULUS MEASUREMENT REPRODUCIBILITY

In the assessment of scan-rescan reproducibility, the within-subject coefficient of variance (CV) was calculated, defined as:

$$\mathrm{CV} = \sqrt{\frac{1}{n}\sum_{i=1}^{n}\frac{\left(\mu_{s(i)}-\mu_{r(i)}\right)^2}{\left(\frac{\mu_{s(i)}+\mu_{r(i)}}{2}\right)^2}} \times 100\ \% \qquad [1]$$

where μ_s is the shear modulus scan measurement, μ_r was the shear modulus rescan measurement, and n was the number of subjects. The within-subject CV was calculated for shear modulus measurements for grey matter, white matter, and the whole brain. The inter-subject CV was calculated by dividing the standard deviation of μ by the mean μ for grey matter, white matter, and whole brain for each three frequencies.

2.5 AIM 2, ASSESSMENT ACROSS MULTIPLE FREQUENCIES

2.5.1 COMPARISON OF SHEAR MODULUS VALUES BETWEEN FREQUENCIES

A one-way analysis of variance (ANOVA) was applied to test for any difference in shear modulus measurements between grey matter, white matter, and whole brain made at all three frequencies. The sum of the squares due to the source (SS), degrees of freedom (df), mean sum of square due to the source (MS), found variation of group averages (F), and expected variations of the group averages (F critical) were calculated for all three frequency groups in white matter, grey matter, and the whole brain region. Pairwise comparisons using Fisher's least significant difference test was performed between frequency measurements for each brain tissue to determine if there was a significant difference.

CHAPTER 3: RESULTS

3.1 SHEAR MODULUS MEASUREMENTS

The mean scan-rescan white matter shear modulus at each frequency for each subject are shown in Table 3.1. The shear modulus for white matter ranged from 4.43 to 2.77 kPa across all three frequencies. The mean grey matter shear modulus at each frequency for each subject are shown in Table 3.2. The shear modulus for grey matter ranged from 1.65 to 3.73 kPa across all three frequencies.

Table 3.1: The average of scan and rescan white matter shear modulus measurements at each frequency for each subject

Subject #	μ at 60 Hz (kPa)	μ at 50 Hz [kPa]	μ at 40 Hz [kPa]
1	3.86	4.22	3.79
2	3.52	3.56	3.28
3	3.26	2.84	2.95
4	3.78	3.86	3.57
5	4.16	3.57	3.20
6	4.10	4.06	3.28
7	3.90	3.91	3.45
8	4.40	4.43	3.77
9	3.41	3.28	2.77
10	4.18	4.03	3.58

Table 3.2: The average of scan and rescan grey matter shear modulus measurements at all three frequencies for each subject

Subject #	μ at 60 Hz (kPa)	μ at 50 Hz [kPa]	μ at 40 Hz [kPa]
1	3.73	3.21	2.61
2	2.91	3.24	2.77
3	2.61	2.25	1.94
4	2.98	2.35	1.91
5	3.22	2.32	1.65
6	4.16	3.55	2.93
7	3.38	2.41	1.73
8	3.35	2.63	2.08
9	3.62	3.30	2.59
10	3.63	3.13	2.18

Table 3.3 shows the mean whole brain shear modulus at each frequency for each subject. The shear modulus for whole brain ranged from 2.38 to 3.56 kPa across all three frequencies. Table 3.4 shows the mean shear modulus of white matter, grey matter, and whole brains for all subjects.

Table 3.3: The average of scan and rescan whole brain shear modulus measurements at all three frequencies for each subject

Subject #	μ at 60 Hz (kPa)	μ at 50 Hz [kPa]	μ at 40 Hz [kPa]
1	3.56	3.26	2.80
2	3.16	2.90	2.38
3	3.16	2.99	2.44
4	3.13	2.91	2.59
5	3.36	2.96	2.57
6	3.52	3.19	2.63
7	3.16	3.01	2.51
8	3.16	3.00	2.61
9	3.22	3.06	2.46
10	3.28	3.10	2.66

The mean white matter shear modulus for all subjects ranged from 3.36 kPa at 40 Hz to 3.85 kPa at 60 Hz. The mean grey matter shear modulus for all subjects ranged from 2.24 kPa at 40 Hz to 3.33 kPa at 60 Hz. For the whole brain, the mean shear modulus for all subjects ranged from 2.57 kPa at 40 Hz to 3.27 kPa at 60 Hz. Boxplots displaying the full range of variation (from minimum to maximum) of shear modulus for white matter and grey matter at a frequency of 60 Hz are shown in Figure 3.1. Figure 3.2 shows the boxplots of shear modulus for white and grey matter at 50 Hz. And for a frequency of 40 Hz, boxplots of shear modulus displaying the full range variation of shear modulus for white and grey matter are shown in Figure 3.3. Wilcoxon signed-rank test indicated that there was a significant statistical difference between white and grey matter shear modulus measurements made at 60 Hz, 50 Hz, and 40 Hz ($P < 0.001$).

Table 3.4: Mean and standard error of shear modulus of white matter, grey matter, and whole brains for all subjects at all three frequencies.

	60 Hz	50 Hz	40 Hz
μ White Matter [kPa]	3.85 ± 0.12	3.78 ± 0.15	3.36 ± 0.11
μ Grey Matter [kPa]	3.33 ± 0.14	2.82 ± 0.16	2.24 ± 0.14
μ Whole Brain [kPa]	3.27 ± 0.05	3.04 ± 0.05	2.57 ± 0.04

At a driver frequency of 60 Hz, the shear modulus of white, grey and whole brain, ranged from 3.26 kPa to 4.40 kPa , 2.61 kPa to 3.73 kPa, 3.13 kPa to 3.56 kPa, respectively. At a driver frequency of 50 Hz, the white matter shear modulus ranged from 2.84 kPa to 4.43 kPa. The shear modulus of grey matter ranged from 2.25 kPa to 3.26 kPa. Whole brain shear modulus ranged from 2.90 kPa to 3.26 kPa. At a driver frequency of 40 Hz, the white matter shear modulus ranged from 2.77 kPa to 3.79 kPa. The grey matter shear modulus ranged from 1.65 kPa to 2.93 kPa. The shear modulus for whole brain ranged from 2.38 kPa to 2.80 kPa. Table 3.5 shows the inter-subject CV for white matter, grey matter, and whole brain shear modulus measurements for each frequency. The inter-subject CV for white matter shear modulus measurements ranged from 10.1% at 40 Hz to 12.4% at 50 Hz. For grey matter shear modulus measurements, the inter-subject CV ranged from 13.1% at 60 Hz to 19.6% at 40 Hz. The inter-subject CVfor whole brain shear modulus measurements ranged from 4.6% at 40 Hz to 4.9% at 50 Hz. The inter-subject CV for grey matter ranged the highest across all frequencies. Grey matter ROIs were the smallest among all regions making it the most challenging region of interest to resolve for all frequencies. Whole brain having the largest ROI among all regions, had the lowest inter-subject CV across all frequencies.

Table 3.5: The inter-subject CV for white matter, grey matter, and whole brain shear modulus measurements for all three frequencies

	60 Hz	50 Hz	40 Hz
White Matter CV %	9.6	12.4	10.1
Grey Matter CV %	13.1	17.7	19.6
Whole Brain CV %	4.8	4.9	4.6

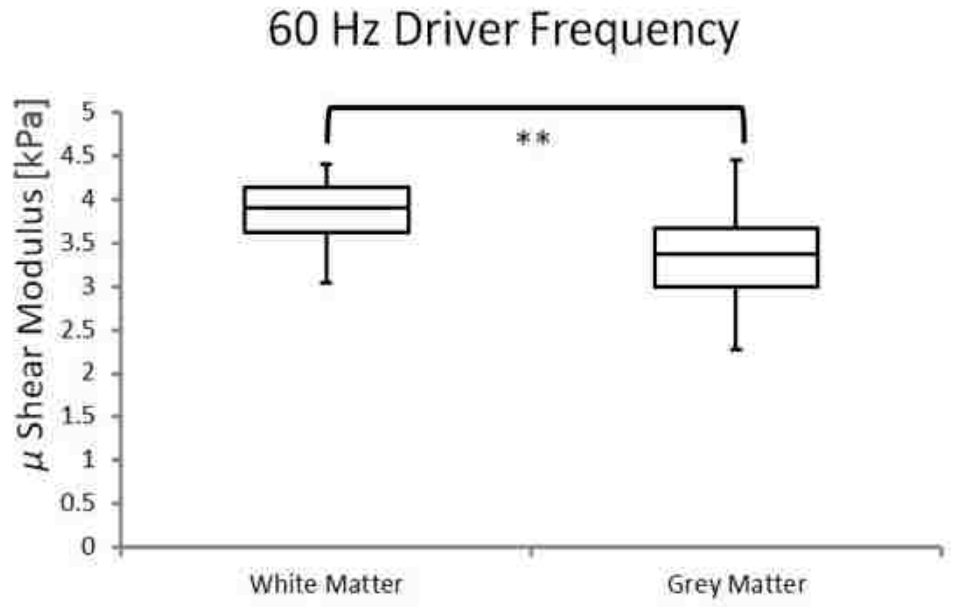

Figure 3.1: Boxplots comparing modulus [kPa] for white and grey matter at 60 Hz. The bottom and the top of the box are the first and third quartile, respectively. The ends of the whiskers represents the minimum and maximum.

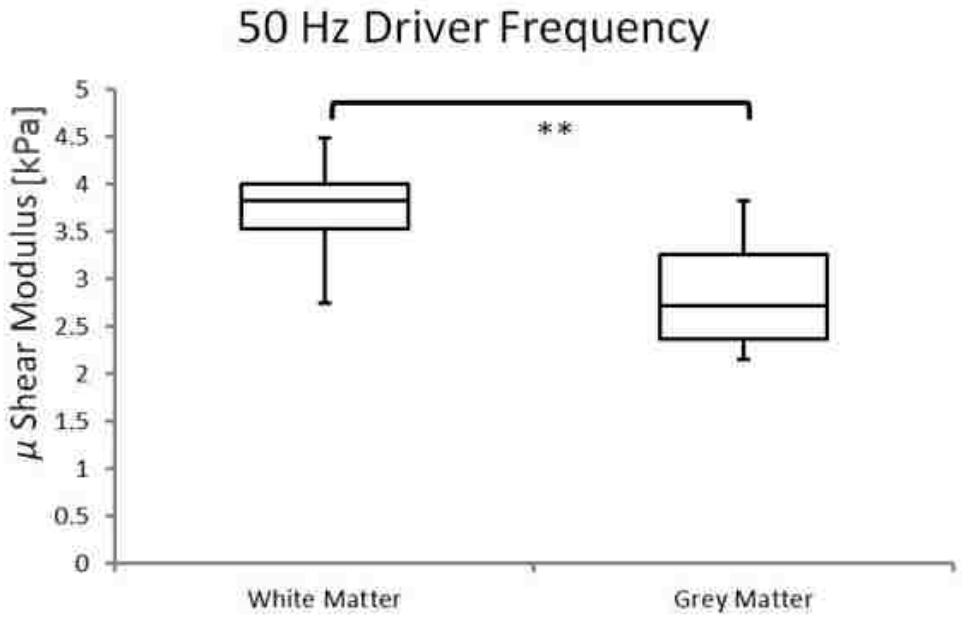

Figure 3.2: Boxplots comparing shear modulus [kPa] for white and grey matter at 50 Hz. The bottom and the top of the box are the first and third quartile, respectively. The ends of the whiskers represents the minimum and maximum.

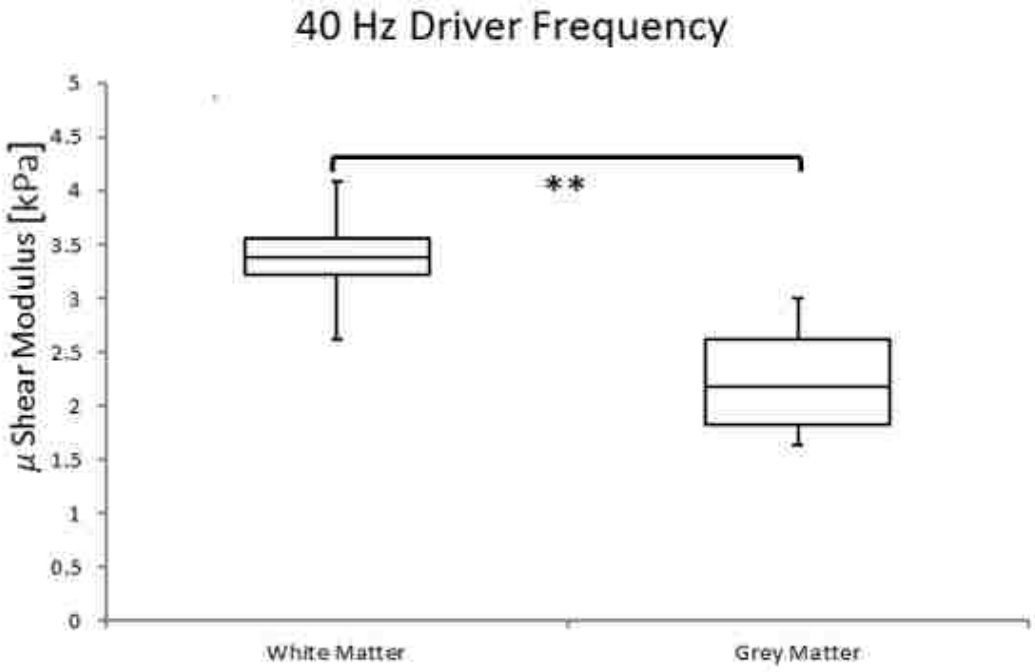

Figure 3.3: Boxplots comparing shear modulus [kPa] for white and grey matter at 40 Hz. The bottom and the top of the box are the first and third quartile, respectively. The ends of the whiskers represents the minimum and maximum.

3.2 RESULTS FOR AIM 1: ASSESSMENT OF SCAN-RESCAN REPRODUCIBILITY

The difference between scan and rescan (Scan-Rescan) shear modulus of white matter, grey matter, and whole brain at 60 Hz are shown in Table 3.6. Scan-Rescan of white matter shear modulus measurements ranged from 0.01 kPa to 0.42 kPa. For grey matter, Scan-Rescan shear modulus measurements ranged from 0.03 kPa to 0.61 kPa. While Scan-Rescan of whole brain shear modulus measurements ranged from 0.01 kPa to 0.23 kPa. The difference of between scan and rescan (Scan-Rescan) shear modulus of white matter, grey matter, and whole brain at 50 Hz are shown in Table 3.7. At 50 Hz, Scan-Rescan of white matter shear modulus measurements ranged from 0.05 kPa to 0.64 kPa. While for grey matter, Scan-Rescan shear modulus measurements ranged from 0.00 kPa to 0.91 kPa at 50 Hz. Whole brain Scan-Rescan shear modulus measurements ranged from 0.01 kPa to 0.55 kPa.

Table 3.6: Difference between scan and rescan (Scan-Rescan) shear modulus of white matter, grey matter, and whole brain at 60 Hz

Subject #	$\Delta\mu$ White Matter Scan – Rescan [kPa]	$\Delta\mu$ Grey Matter Scan-Rescan [kPa]	$\Delta\mu$ Whole Brain Scan-Rescan [kPa]
1	0.42	0.06	0.19
2	0.34	0.03	0.08
3	0.42	0.66	0.17
4	0.01	0.08	0.15
5	0.03	0.10	0.06
6	0.13	0.61	0.04
7	0.35	0.06	0.11
8	0.01	0.23	0.01
9	0.27	0.08	0.23
10	0.07	0.21	0.16

Table 3.7: Difference between scan and rescan (Scan-Rescan) shear modulus of white matter, grey matter, and whole brain at 50 Hz

Subject #	$\Delta\mu$ White Matter Scan – Rescan [kPa]	$\Delta\mu$ Grey Matter Scan-Rescan [kPa]	$\Delta\mu$ Whole Brain Scan-Rescan [kPa]
1	0.54	0.09	0.10
2	0.11	0.16	0.04
3	0.19	0.19	0.10
4	0.18	0.19	0.02
5	0.06	0.00	0.01
6	0.20	0.55	0.28
7	0.05	0.08	0.21
8	0.12	0.27	0.06
9	0.35	0.21	0.13
10	0.64	0.91	0.55

The difference of between scan and rescan (Scan-Rescan) shear modulus of white matter, grey matter, and whole brain at 40 Hz are shown in Table 3.8. At 40 Hz, Scan-Rescan of white matter shear modulus measurements ranged from 0.01 kPa to 0.60 kPa. While for grey matter, Scan-Rescan shear modulus measurements ranged from 0.03 kPa to 0.46 kPa at 40 Hz. Whole brain Scan-Rescan shear modulus measurements ranged from 0.01 kPa to 0.19 kPa at 40 Hz. Figure 3.4 shows a Bland-Altman plot of the difference between scan and rescan white matter

shear modulus measurements vs their average at 60 Hz. The mean difference between scan and rescan white matter shear modulus measurements was 0.06 kPa. The coefficient of reproducibility was 0.53, and all differences between scan and rescan white matter shear modulus measurements at 60 Hz were less than two standard deviations. The data appears to be normally distributed. There does not appear to be any relation between difference of Scan-Rescan white matter shear modulus measurements and the magnitude of their average at 60 Hz. Meaning that there wasn't a significant statistical difference from a zero difference.

Figure 3.5 shows a Bland-Altman plot of the difference between scan and rescan white matter shear modulus measurements vs their average at 50 Hz. The mean difference between scan and rescan white matter shear modulus measurements was -0.02 kPa. The coefficient of reproducibility was 0.64, and all differences between scan and rescan white matter shear modulus measurements at 50 Hz except for one, were less than two standard deviations. There does not appear to be any relation between difference of Scan-Rescan white matter shear modulus measurements and the magnitude of their average at 50 Hz. There wasn't a significant statistical difference from a difference of zero. Figure 3.6 shows a Bland-Altman plot of the difference between scan and rescan white matter shear modulus measurements vs their average at 40 Hz. The mean difference between scan and rescan white matter shear modulus measurements was -0.05 kPa. The coefficient of reproducibility was 0.50, and all differences between scan and rescan white matter shear modulus measurements at 40 Hz except for one, were less than two standard deviations. There does not appear to be any relation between difference of Scan-Rescan white matter shear modulus measurements and the magnitude of their average at 40 Hz. There wasn't a significant statistical difference from a difference of zero.

Table 3.8: Difference between scan and rescan (Scan-Rescan) shear modulus of white matter, grey matter, and whole brain at 40 Hz

Subject #	$\Delta\mu$ White Matter Scan – Rescan [kPa]	$\Delta\mu$ Grey Matter Scan-Rescan [kPa]	$\Delta\mu$ Whole Brain Scan-Rescan [kPa]
1	0.60	0.15	0.19
2	0.04	0.08	0.10
3	0.32	0.09	0.07
4	0.09	0.30	0.11
5	0.07	0.03	0.03
6	0.07	0.15	0.04
7	0.01	0.08	0.11
8	0.11	0.46	0.01
9	0.31	0.03	0.03
10	0.08	0.13	0.07

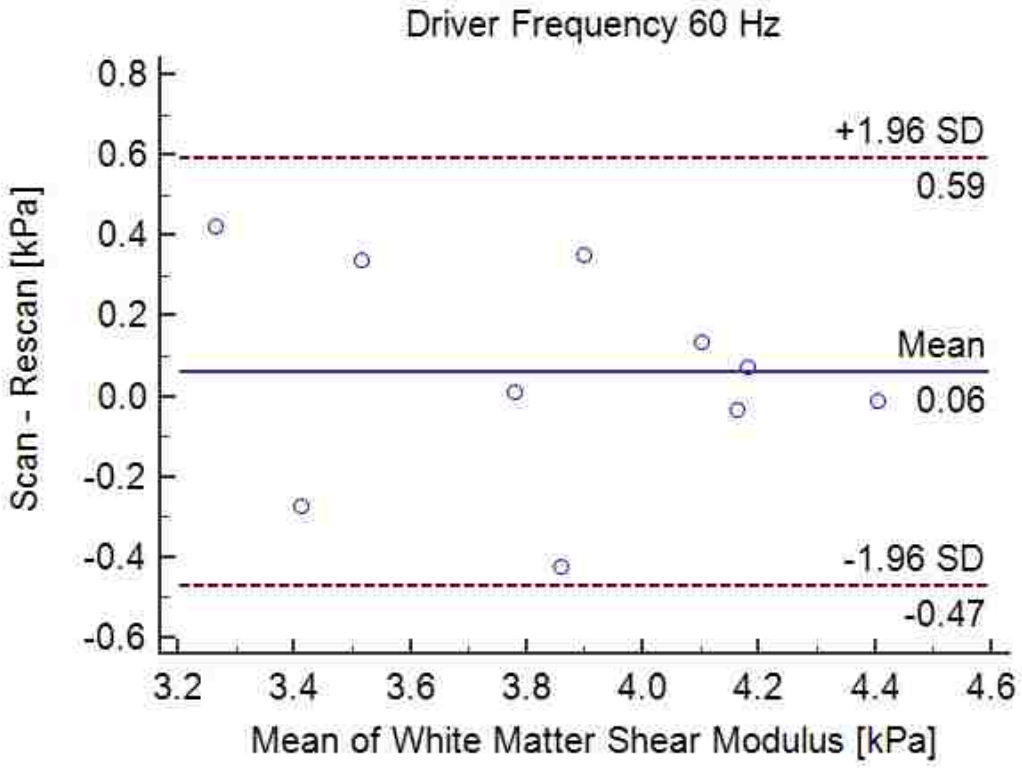

Figure 3.4: Bland-Altman plot of the difference between scan and rescan white matter shear modulus measurements vs their averages at 60 Hz (SD, standard deviation).

Figure 3.7 shows a Bland-Altman plot of the difference between scan and rescan grey matter shear modulus measurements vs their average at 60 Hz. The mean difference between scan and rescan grey matter shear modulus measurements was 0.11 kPa. The coefficient of reproducibility was 0.59, and all differences between scan and rescan grey matter shear modulus measurements at 60 Hz were less than two standard deviations. At 60 Hz, The difference of Scan-Rescan grey matter shear modulus measurements shows no dependence on the magnitude of their average. There wasn't a significant statistical difference from a difference of zero

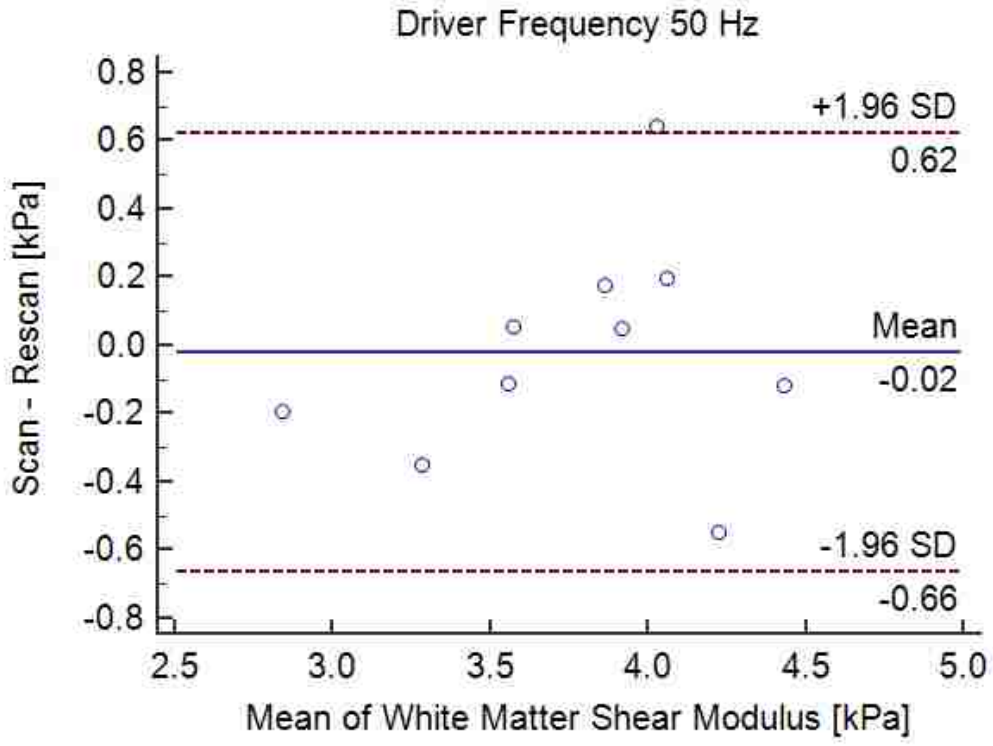

Figure 3.5: Bland-Altman plot Bland-Altman plot of the difference between scan and rescan white matter shear modulus measurements vs their averages at 50 Hz (SD, standard deviation).

Figure 3.8 shows a Bland-Altman plot of the difference between scan and rescan grey matter shear modulus measurements vs their average at 50 Hz. The mean difference between scan and rescan grey matter shear modulus measurements was -0.15 kPa. The coefficient of reproducibility was 0.70, and all differences between scan and rescan grey matter shear modulus

measurements at 50 Hz except for one, were less than two standard deviations. At 50 Hz, The difference of Scan-Rescan grey matter shear modulus measurements shows no dependence on the magnitude of their average.

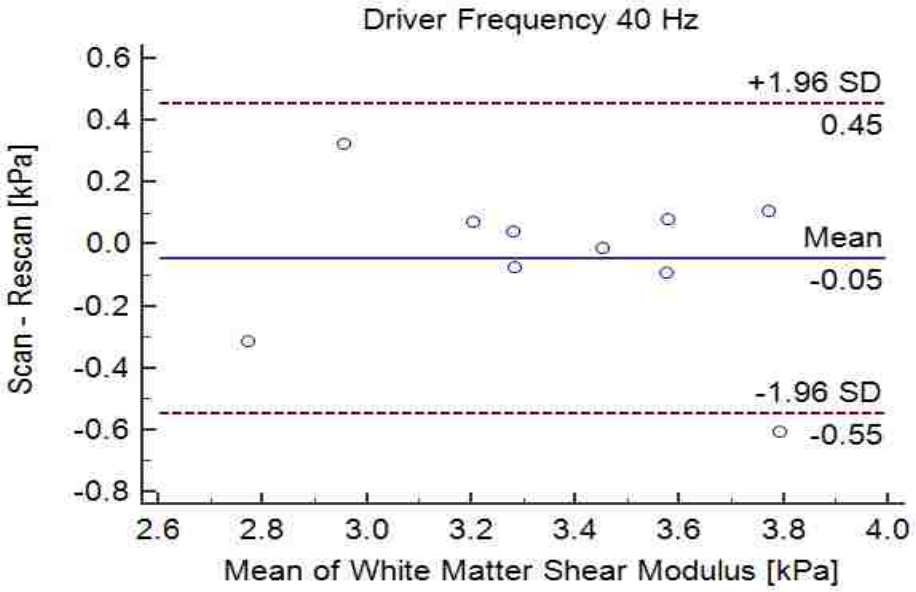

Figure 3.6: Bland-Altman plot Bland-Altman plot of the difference between scan and rescan white matter shear modulus measurements vs their averages at 40 Hz (SD, standard deviation).

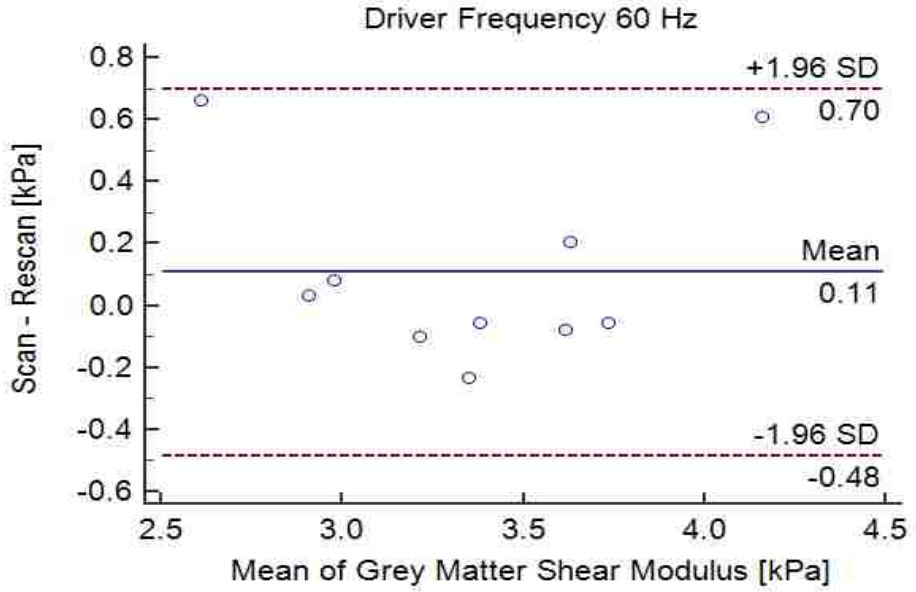

Figure 3.7: Bland-Altman plot Bland-Altman plot of the difference between scan and rescan grey matter shear modulus measurements vs their averages at 60 Hz (SD, standard deviation).

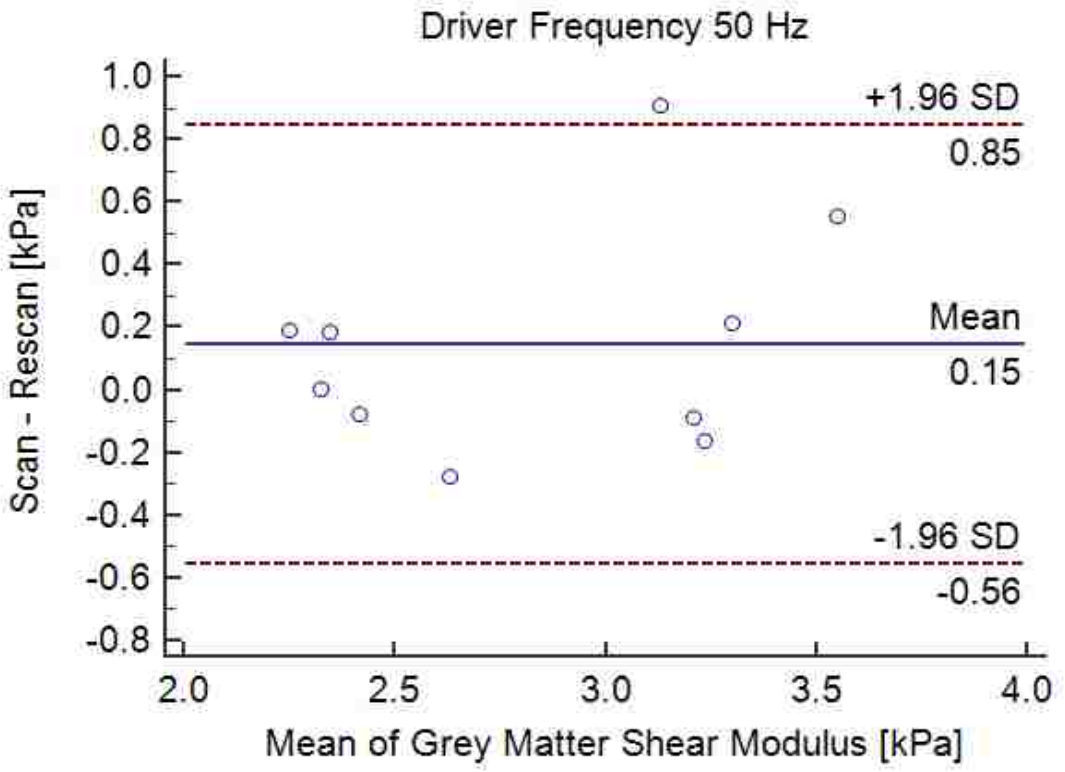

Figure 3.8: Bland-Altman plot Bland-Altman plot of the difference between scan and rescan grey matter shear modulus measurements vs their averages at 50 Hz (SD, standard deviation).

Figure 3.9 shows a Bland-Altman plot of the difference between scan and rescan grey matter shear modulus measurements vs their average at 40 Hz. The mean difference between scan and rescan grey matter shear modulus measurements was -0.02 kPa. The coefficient of reproducibility was 0.40, and all differences between scan and rescan grey matter shear modulus measurements at 40 Hz but one were less than two standard deviations. The data appears to be normally distributed. At 40 Hz, The difference of Scan-Rescan grey matter shear modulus measurements shows no dependence on the magnitude of their average. There wasn't a significant statistical difference from a difference of zero. Even though grey matter had the smallest ROIs among all regions, high reproducibility was observed between scan and rescan measurements.

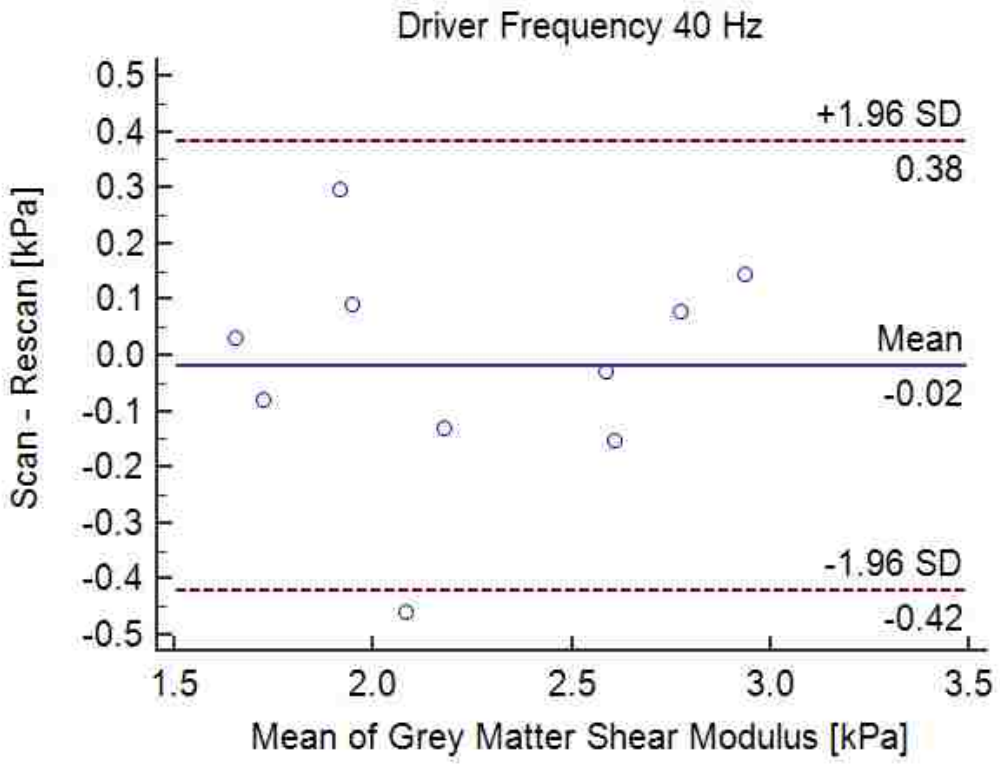

Figure 3.9: Bland-Altman plot Bland-Altman plot of the difference between scan and rescan grey matter shear modulus measurements vs their averages at 40 Hz (SD, standard deviation).

Figure 3.10 shows a Bland-Altman plot of the difference between scan and rescan whole brain shear modulus measurements vs their average at 60 Hz. The mean difference between scan and rescan whole brain shear modulus measurements was 0.01 kPa. The coefficient of reproducibility was 0.28, and all differences between scan and rescan whole brain shear modulus measurements at 60 Hz were less than two standard deviations. The data appears to be normally distributed. There does not appear to be any relation between difference of Scan-Rescan whole brain shear modulus measurements and the magnitude of their average at 60 Hz. There wasn't a significant statistical difference from a difference of zero. The data indicates that whole brain shear modulus measurements at 60 Hz are highly reproducible.

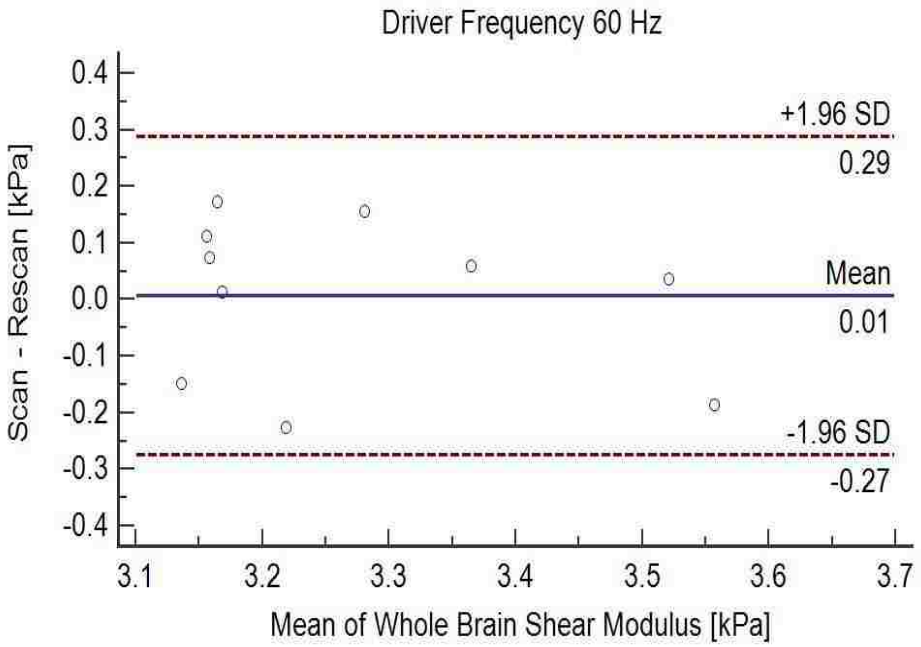

Figure 3.10: Bland-Altman plot Bland-Altman plot of the difference between scan and rescan whole brain shear modulus measurements vs their averages at 60 Hz (SD, standard deviation).

Figure 3.11 shows a Bland-Altman plot of the difference between scan and rescan whole brain shear modulus measurements vs their average at 50 Hz. The mean difference between scan and rescan whole brain shear modulus measurements was 0.08 kPa. The coefficient of reproducibility was 0.41, and all differences between scan and rescan whole brain shear modulus measurements at 50 Hz except for one, were less than two standard deviations. There does not appear to be any relation between difference of Scan-Rescan whole brain shear modulus measurements and the magnitude of their average at 50 Hz. There wasn't a significant statistical difference from a difference of zero. Figure 3.12 shows a Bland-Altman plot of the difference between scan and rescan whole brain shear modulus measurements vs their average at 40 Hz. The mean difference between scan and rescan whole brain shear modulus measurements was 0.01 kPa. The coefficient of reproducibility was 0.19, and all differences between scan and rescan whole brain shear modulus measurements at 40 Hz except for one, were less than two standard deviations. There does not appear to be any relation between difference of Scan-Rescan

whole brain shear modulus measurements and the magnitude of their average at 40 Hz. There wasn't a significant statistical difference from a difference of zero.

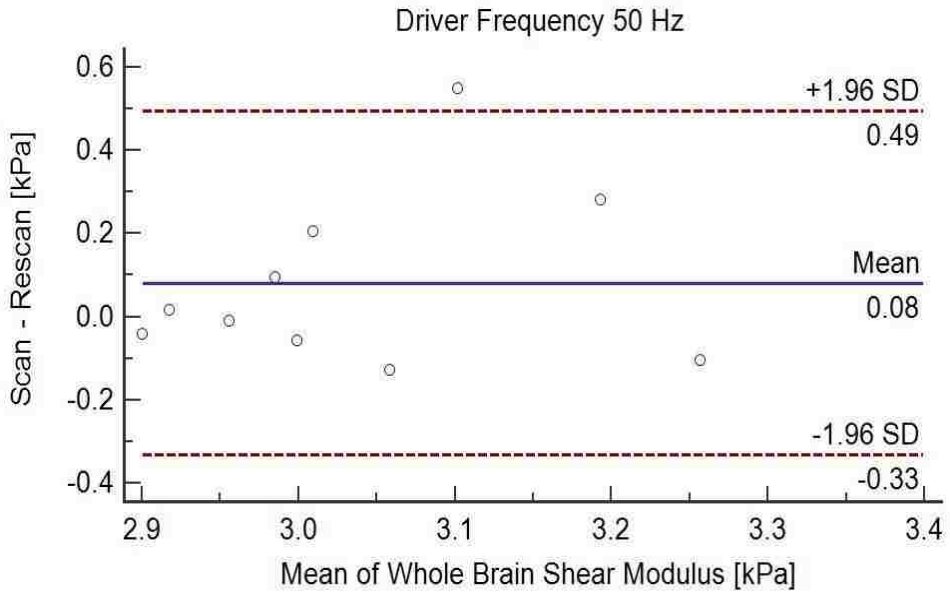

Figure 3.11: Bland-Altman plot Bland-Altman plot of the difference between scan and rescan whole brain shear modulus measurements vs their averages at 50 Hz (SD, standard deviation).

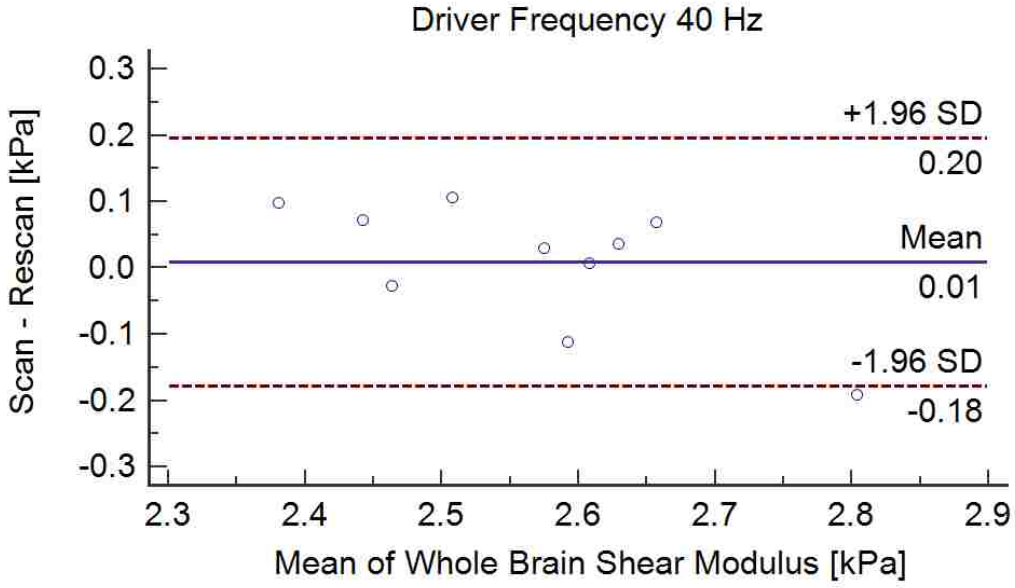

Figure 3.12: Bland-Altman plot Bland-Altman plot of the difference between scan and rescan whole brain shear modulus measurements vs their averages at 40 Hz (SD, standard deviation).

The Within-subject coefficients of variance at driver frequencies of 60, 50, and 40 Hz are listed in Table 3.9. The within-subject coefficient of variance for white matter shear modulus measurements ranged from 3.7 % at 60 Hz to 4.1 % at 50 Hz. For grey matter, the coefficient of variance for shear modulus measurements ranged from 4.7% at 60 Hz to 6.0 % at 50 Hz. The within-subject coefficient of variance for whole brain shear modulus measurements ranged from 1.8 % at 40 Hz to 3.5 % at 60Hz.

Table 3.9: The within-subject coefficients of variance at driver frequencies of 60, 50, and 40 Hz (coefficient of variance)

	60 Hz	50 Hz	40 Hz
White Matter CV %	3.7	4.1	3.9
Grey Matter CV %	4.9	6.0	4.7
Whole Brain CV %	2.1	3.5	1.8

3.3 RESULTS FOR AIM 2: ASSESSMENT ACROSS MULTIPLE FREQUENCIES

An ANOVA was performed to test the following null hypothesis: frequency had no effect on shear modulus measurements (H_0:$\mu_{60\ Hz} = \mu_{50\ Hz} = \mu_{40\ Hz}$.). Table 3.10 summarizes the ANOVA results for white matter, grey matter, and whole brain. The found variation of the group averages (F) of different frequencies was found to be greater than the expected variation (F critical) for white matter, grey matter, and whole brain. This indicates that we must reject the null hypothesis. The ANOVA results indicates that at least one frequency is significantly different from the other two.

Table 3.10: Analysis of variance results of white matter, grey matter, and whole brain (SS, The sum of squares due to the source; MS, the mean sum of squares due to the source; F, found variation of the group averages; F critical, expected variation of the group averages)

Source of Variation	SS	df	MS	F	P-value	F critical
Frequency in White Matter	2.03	2	1.02	17.54	P <0.001	3.55
Frequency in Grey Matter	6.26	2	3.13	51.58	P <0.001	3.55
Frequency in Whole Brain	2.59	2	1.29	283.92	P <0.001	3.55

Pairwise comparisons using Fisher's least significant difference test was performed between frequency measurements for each brain tissue to determine if there was a significant difference. For grey matter, and whole brain, all the frequencies were significantly different from one another. For white matter, the stiffness at 40 Hz was significantly different from that at 60 Hz. For white matter, the stiffness at 50 Hz was not significantly different from those at 40 Hz or 60 Hz. The passive driver's vibrational mode at 50 Hz, could have behave differently than at 60 Hz and 40 Hz.

CHAPTER 4: DISCUSSION AND CONCLUSIONS

4.1 DRIVER PERFORMANCE AND SHEAR MODULUS MEASUREMENTS

The wave images for all subjects showed induced shear wave propagation in the regions of interest, at all three frequencies (Appendix A). This indicated that the ergonomic flexible driver successfully induced shear propagation in the brain. None of the subjects reported discomfort due to the passive driver. Attenuation of the shear waves increased with frequency (Appendix A). A significant statistical difference was found between the measured shear modulus of white and grey matter. The shear modulus of white matter was found to be higher in than that of grey matter. This agrees with the published literature that white matter. The average shear modulus values of white and grey matter measured in this study were in the lower range of the reported in Table 1.1.The whole brain shear modulus at 60 Hz was 3.27 ± 0.16 kPa; Murphy et al. reported a whole brain shear modulus value of 3.01 kPa (Murphy, Huston et al. 2011). This disagreement likely was due to differences in the median age of the population and the ratio of female to male subjects in this study. Arani et al. reported there is brain softening that occurs with aging, and stiffness differences due to gender exist in the temporal and occipital lobes (Arani, Murphy et al. 2015).

4.2 AIM 1 DISCUSSION

Scan-Rescan reproducibility was assessed in all three regions of interests, at all frequencies. No observed relationship was observed between the difference of scan and rescan measurements and their average for all regions of interests, at all frequencies. The Bland-Altman plots indicated good reproducibility at all frequencies. The within-subject coefficient of variance was below 6% for white matter, grey matter, and the whole brain. This indicated that the shear modulus was a highly reproducible imaging biomarker.

4.3 AIM 2 DISCUSSION

The shear modulus was shown previously to be frequency-independent in tissue mimicking phantoms (Hamhaber, Grieshaber et al. 2003). Analysis of variance was performed to test if there were any differences between measurements made at different frequencies. The results of the analysis of variance indicated that the shear modulus measurements in the brain were frequency dependent. The shear modulus also seemed to be increasing with driver frequency (see Table 3.4 and the elastograms in Appendix B).

4.4 LIMITATIONS

A potential limitation of this study was subject population age, ranging from 24 to 38 yrs. A second limitation was wave propagation was only encoded along one dimension. This made it difficult to determine the true shear stiffness of brain tissue because the displacement in the other two dimensions was unaccounted for. Brain tissue is somewhay anisotropic, and the white matter tracts may act as wave guides for the propagating shear waves (Romano, Scheel et al. 2012). The algorithm that was used to reconstruct elastograms in this study assumed isotropic material. Failure to account for anisotropy might result in an uncertainty of the shear modulus in brain tissue. The driver couldn't operate at frequencies higher than 60 Hz because of an intense increase in attenuation. Higher frequencies would provide a more optimal resolution when performing MRE of the brain.

4.5 FUTURE WORK

Radiation necrosis is a severe post-treatment local tissue reaction with disruption to the blood brain barrier (BBB), with evidence of edema, and necrosis, with or without mass effect on MRI (O'Brien and Colen 2014). Cerebral radiation-induced necrosis manifests itself at radiotherapy doses of less than 50 Gy and increases with increasing fraction dose, fraction size,

and the administration of chemotherapy (Ruben, Dally et al. 2006). Neuroimages of late cerebral radiation-induced necrosis do not consistently show a definite finding. Many cases of cerebral radiation necrosis show enhancement with the administration of gadolinium-diethylenetriamine pentaacetic acid (Gd-DTPA) contrast agent on MRI examination, however some cases do not show any enhancement (Yoshii 2008). Currently, there are no standardized imaging methods for reliably differentiating radiation necrosis from high-grade glioma recurrence (Fink, Born et al. 2012). MRE can potentially be used to differentiate radiation induced necrosis from tumor recurrence.

In future work, a larger subject population should be studied. Three dimensional MRE is recommended to allow the reconstruction of elastograms using the full AIDE algorithm, which is expected to yield more accurate results. Combining diffusion tensor imaging with MRE, would allow for the assessment of the anisotropic mechanical properties of biological tissue (Qin, Sinkus et al. 2013). Passive drivers should be designed to operate at higher frequencies with a minimal amount of attenuation. Investigating how different component materials of the passive driver affect its performance, would allow for its optimization. A high spatial resolution due to mechanical frequency is necessary in order to be able to differentiate normal brain tissue from malignancies (Xu, Lin et al. 2007).

4.6 CONCLUSION

This study demonstrated the ability to make in vivo shear modulus measurements of brain tissue. MRE with the brain-compatible driver was able to differentiate white matter from grey matter. The white and grey matter shear modulus values measured in this study were within the range of values reported in literature. Shear modulus has the potential to be used as a biomarker in order to differentiate normal tissue from malignancies. Shear modulus

measurements with the brain-compatible driver exhibited a frequency dependence. This shows the importance of standardizing MRE imaging parameters to facilitate the use of this technique in the clinic. An assessment of reproducibility was performed. Shear modulus as a biomarker displayed a low within-subject coefficient of variance, indicating a high level of reproducibility.

REFERENCES

Arani, A., M. C. Murphy, K. J. Glaser, A. Manduca, D. S. Lake, S. A. Kruse, C. R. Jack, Jr., R. L. Ehman and J. Huston, 3rd (2015). "Measuring the effects of aging and sex on regional brain stiffness with MR elastography in healthy older adults." NeuroImage **111**: 59-64.

Bravo, A. A., S. G. Sheth and S. Chopra (2001). "Liver biopsy." N Engl J Med **344**(7): 495-500.

Di Ieva, A., F. Grizzi, E. Rognone, Z. T. H. Tse, T. Parittotokkaporn, F. Rodriguez y Baena, M. Tschabitscher, C. Matula, S. Trattnig and R. R. Y. Baena (2010). "Magnetic resonance elastography: a general overview of its current and future applications in brain imaging." Neurosurgical Review **33**(2): 137-145.

Ehman, E. C., P. J. Rossman, S. A. Kruse, A. V. Sahakian and K. J. Glaser (2008). "Vibration safety limits for magnetic resonance elastography." Physics in Medicine and Biology **53**(4): 925-935.

Fink, J., D. Born and M. C. Chamberlain (2012). "Radiation Necrosis: Relevance with Respect to Treatment of Primary and Secondary Brain Tumors." Current Neurology and Neuroscience Reports **12**(3): 276-285.

Hamhaber, U., V. A. Grieshaber, J. H. Nagel and U. Klose (2003). "Comparison of quantitative shear wave MR-elastography with mechanical compression tests." Magnetic Resonance in Medicine **49**(1): 71-77.

Hernandez-Gea, V. and S. L. Friedman (2011). "Pathogenesis of Liver Fibrosis." Annual Review of Pathology: Mechanisms of Disease, Vol 6 **6**: 425-456.

Kim, W. R., R. S. Brown, N. A. Terrault and H. El-Serag (2002). "Burden of liver disease in the United States: Summary of a workshop." Hepatology **36**(1): 227-242.

Manduca, A., T. E. Oliphant, M. A. Dresner, J. L. Mahowald, S. A. Kruse, E. Amromin, J. P. Felmlee, J. F. Greenleaf and R. L. Ehman (2001). "Magnetic resonance elastography: Non-invasive mapping of tissue elasticity." Medical Image Analysis **5**(4): 237-254.

Mariappan, Y. K., K. J. Glaser and R. L. Ehman (2010). "Magnetic resonance elastography: a review." Clin Anat **23**(5): 497-511.

Muller, G. (2007). Theory of Elastic Waves. Germany, Samizdat Press.

Murphy, M. C., J. Huston, 3rd, C. R. Jack, Jr., K. J. Glaser, A. Manduca, J. P. Felmlee and R. L. Ehman (2011). "Decreased brain stiffness in Alzheimer's disease determined by magnetic resonance elastography." J Magn Reson Imaging **34**(3): 494-498.

Muthupillai, R., D. J. Lomas, P. J. Rossman, J. F. Greenleaf, A. Manduca and R. L. Ehman (1995). "Magnetic-Resonance Elastography by Direct Visualization of Propagating Acoustic Strain Waves." Science **269**(5232): 1854-1857.

O'Brien, B. J. and R. R. Colen (2014). "Post-Treatment Imaging Changes in Primary Brain Tumors." Current Oncology Reports **16**(8).

Oliphant, T. E., A. Manduca, R. L. Ehman and J. F. Greenleaf (2001). "Complex-valued stiffness reconstruction for magnetic resonance elastography by algebraic inversion of the differential equation." Magnetic Resonance in Medicine **45**(2): 299-310.

Qin, E. C., R. Sinkus, G. Q. Geng, S. Cheng, M. Green, C. D. Rae and L. E. Bilston (2013). "Combining MR elastography and diffusion tensor imaging for the assessment of anisotropic mechanical properties: A phantom study." Journal of Magnetic Resonance Imaging **37**(1): 217-226.

Romano, A., M. Scheel, S. Hirsch, J. Braun and I. Sack (2012). "In vivo waveguide elastography of white matter tracts in the human brain." Magnetic Resonance in Medicine **68**(5): 1410-1422.

Ruben, J. D., M. Dally, M. Bailey, R. Smith, C. A. McLean and P. Fedele (2006). "Cerebral radiation necrosis: incidence, outcomes, and risk factors with emphasis on radiation parameters and chemotherapy." Int J Radiat Oncol Biol Phys **65**(2): 499-508.

Shi, Y., K. J. Glaser, S. K. Venkatesh, E. I. Ben-Abraham and R. L. Ehman (2015). "Feasibility of Using 3D MR Elastography to Determine Pancreatic Stiffness in Healthy Volunteers." Journal of Magnetic Resonance Imaging **41**(2): 369-375.

Streitberger, K. J., F. Paul, D. Krefting, D. Klatt, S. Papazoglou , S. Hirsch, J. Braun and I. Sack (2010). Decrease of brain stiffness compared to loss of brain volume in Multiple Sclerosis patients Proceedings of the 18th Annual Meeting of ISMRM,. **18**.

Venkatesh, S. K., M. Yin, J. F. Glockner, N. Takahashi, P. A. Araoz, J. A. Talwalkar and R. L. Ehman (2008). "MR elastography of liver tumors: Preliminary results." American Journal of Roentgenology **190**(6): 1534-1540.

Xu, L., Y. Lin, J. C. Han, Z. N. Xi, H. Shen and P. Y. Gao (2007). "Magnetic resonance elastography of brain tumors: Preliminary results." Acta Radiologica **48**(3): 327-330.

Yin, M., J. A. Talwalkar, K. J. Glaser, A. Manduca, R. C. Grimm, P. J. Rossman, J. L. Fidler and R. L. Ehman (2007). "Assessment of hepatic fibrosis with magnetic resonance elastography." Clin Gastroenterol Hepatol **5**(10): 1207-1213 e1202.

Yoshii, Y. (2008). "Pathological review of late cerebral radionecrosis." Brain Tumor Pathology **25**(2): 51-58.

APPENDIX A: WAVE IMAGES FOR ALL SUBJECTS

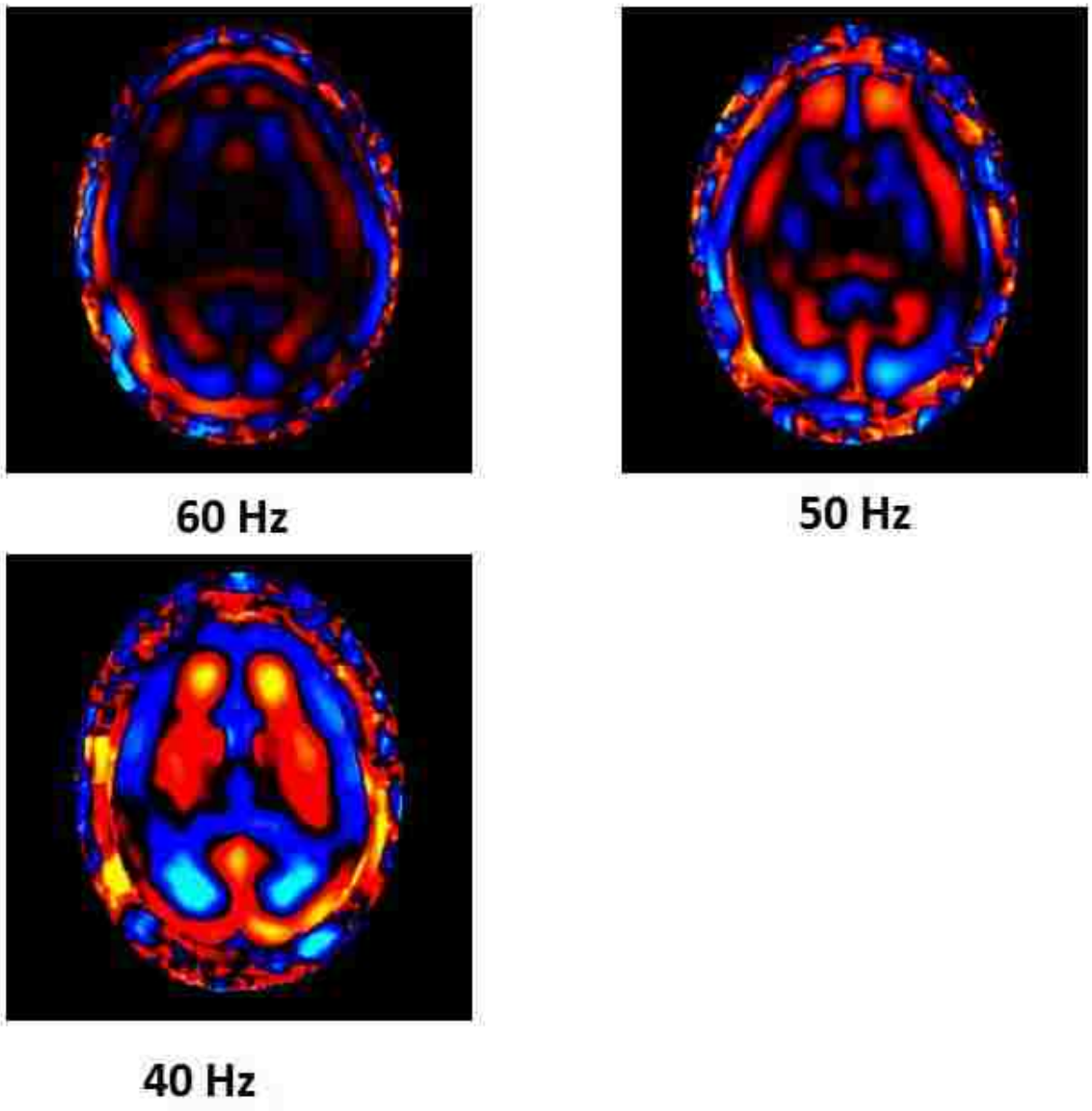

Figure A.1: Scan wave images for Subject 1 at 60 Hz (upper right), 50 Hz (upper left), and 40 Hz (bottom right).

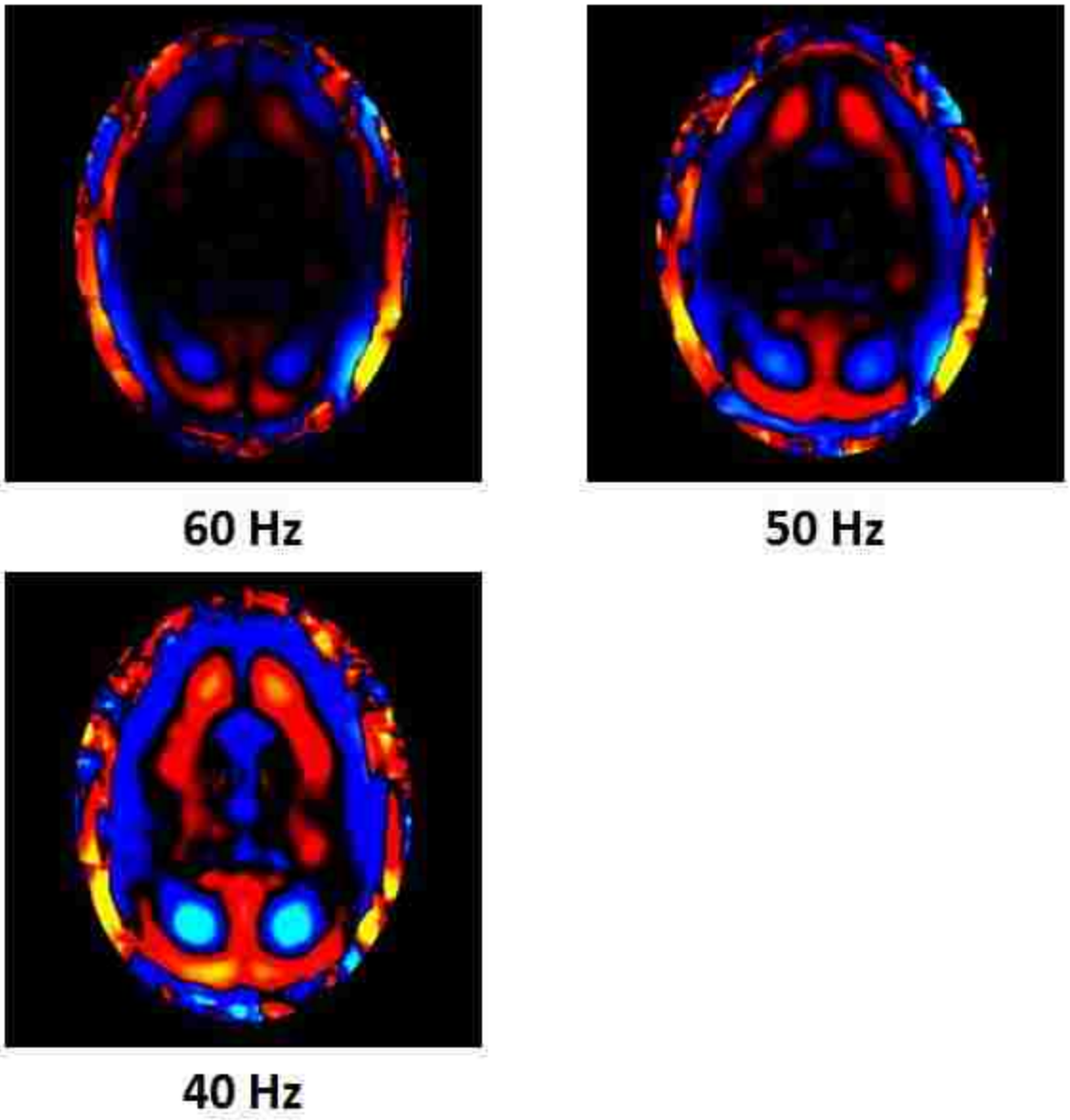

Figure A.2: Scan wave images for Subject 2 at 60 Hz (upper right), 50 Hz (upper left), and 40 Hz (bottom right).

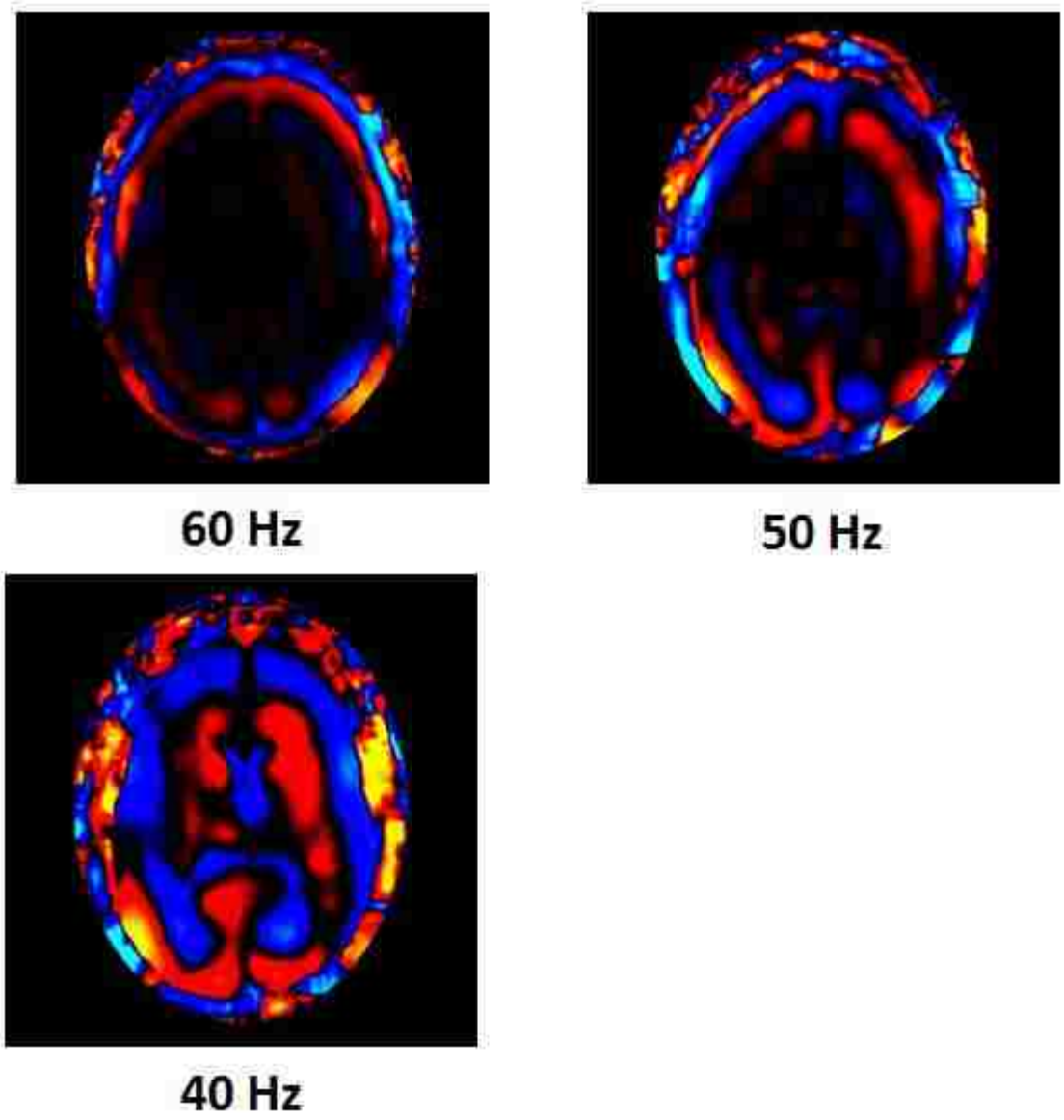

Figure A.3: Scan wave images for subject 3 at 60 Hz (upper Right), 50 Hz (upper left), and 40 Hz (bottom right).

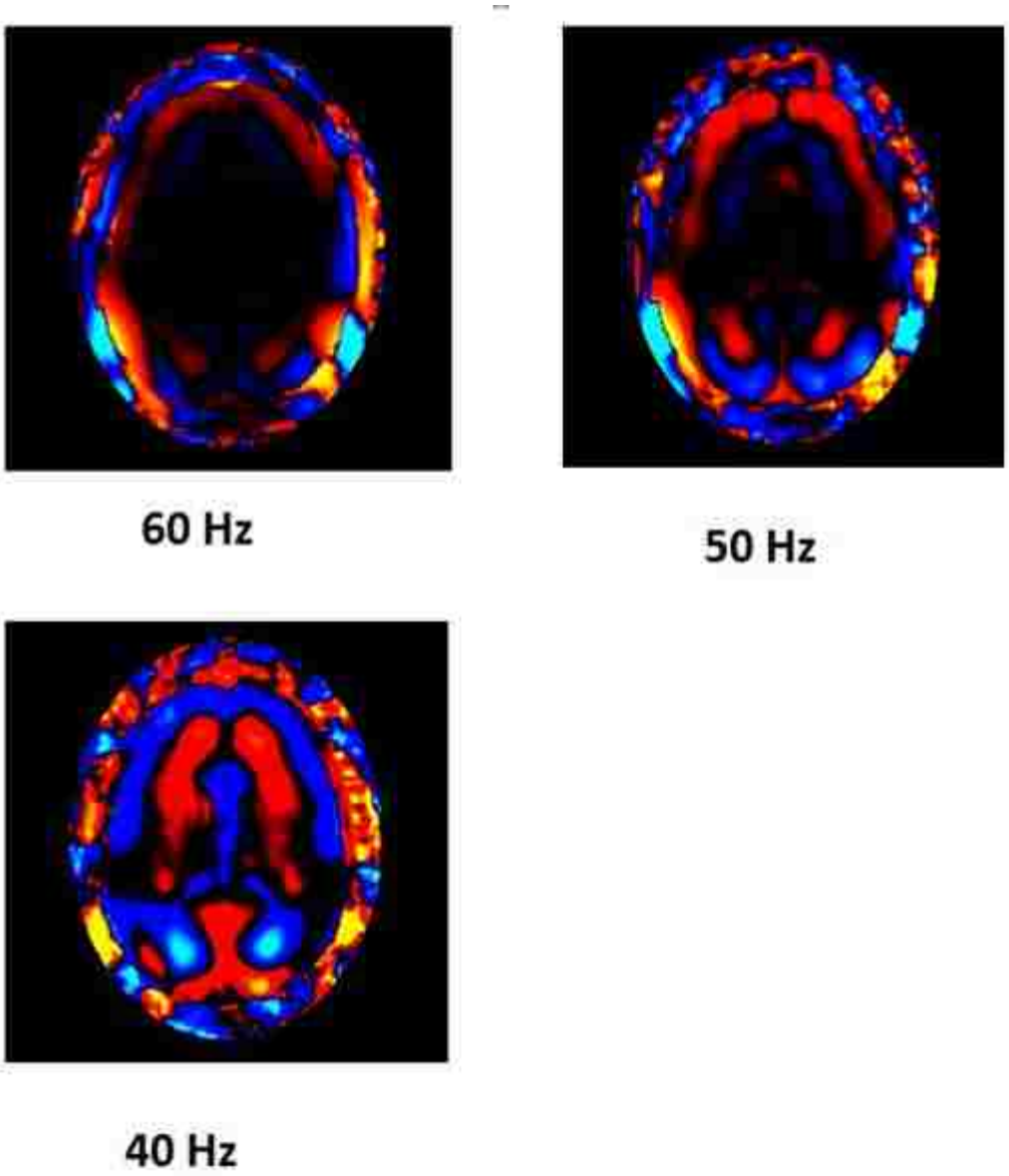

Figure A.4: Scan wave images for subject 4 at 60 Hz (upper Right), 50 Hz (upper left), and 40 Hz (bottom right).

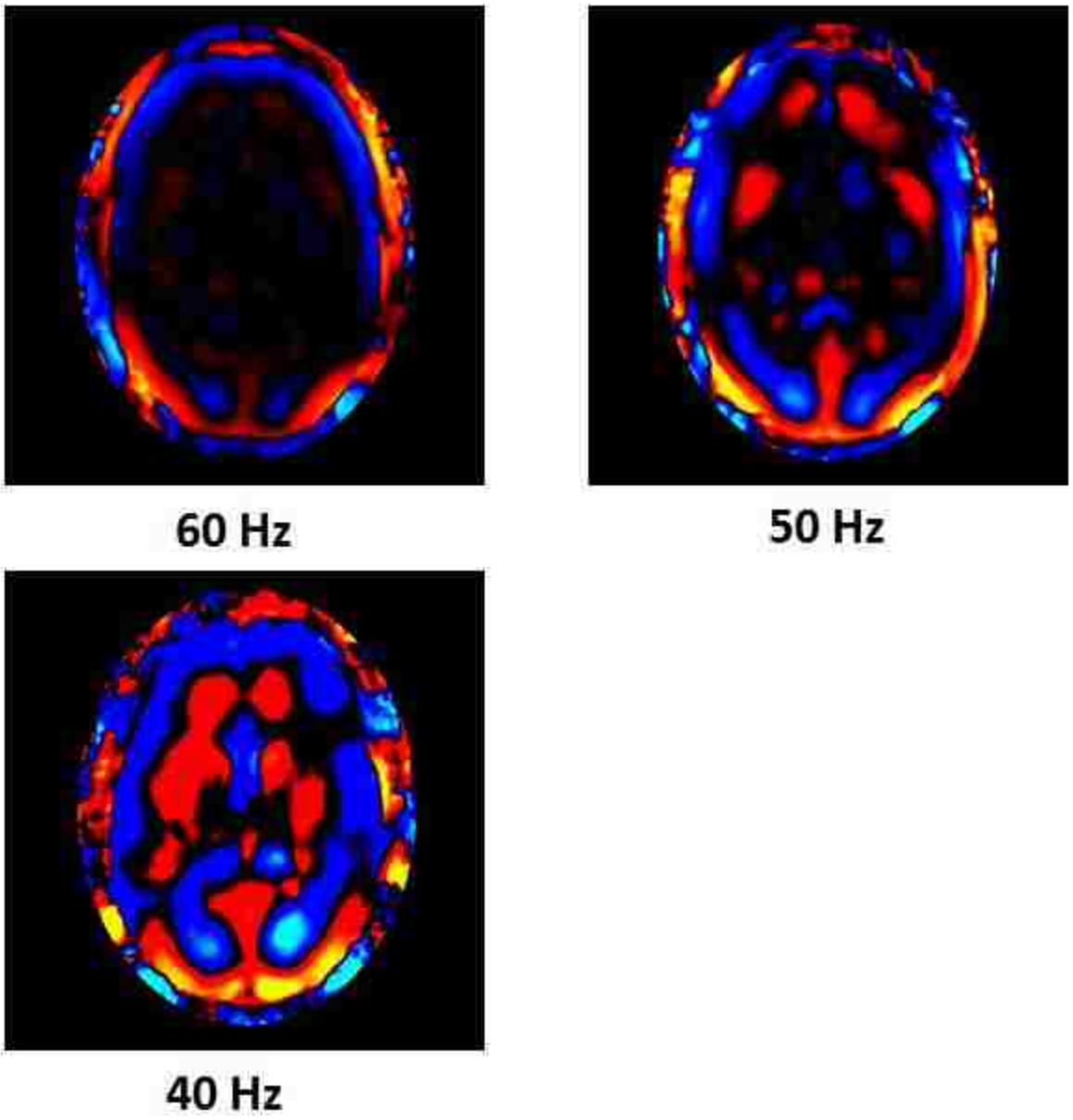

Figure A.5: Scan wave images for Subject 5 at 60 Hz (upper right), 50 Hz (upper left), and 40 Hz (bottom right).

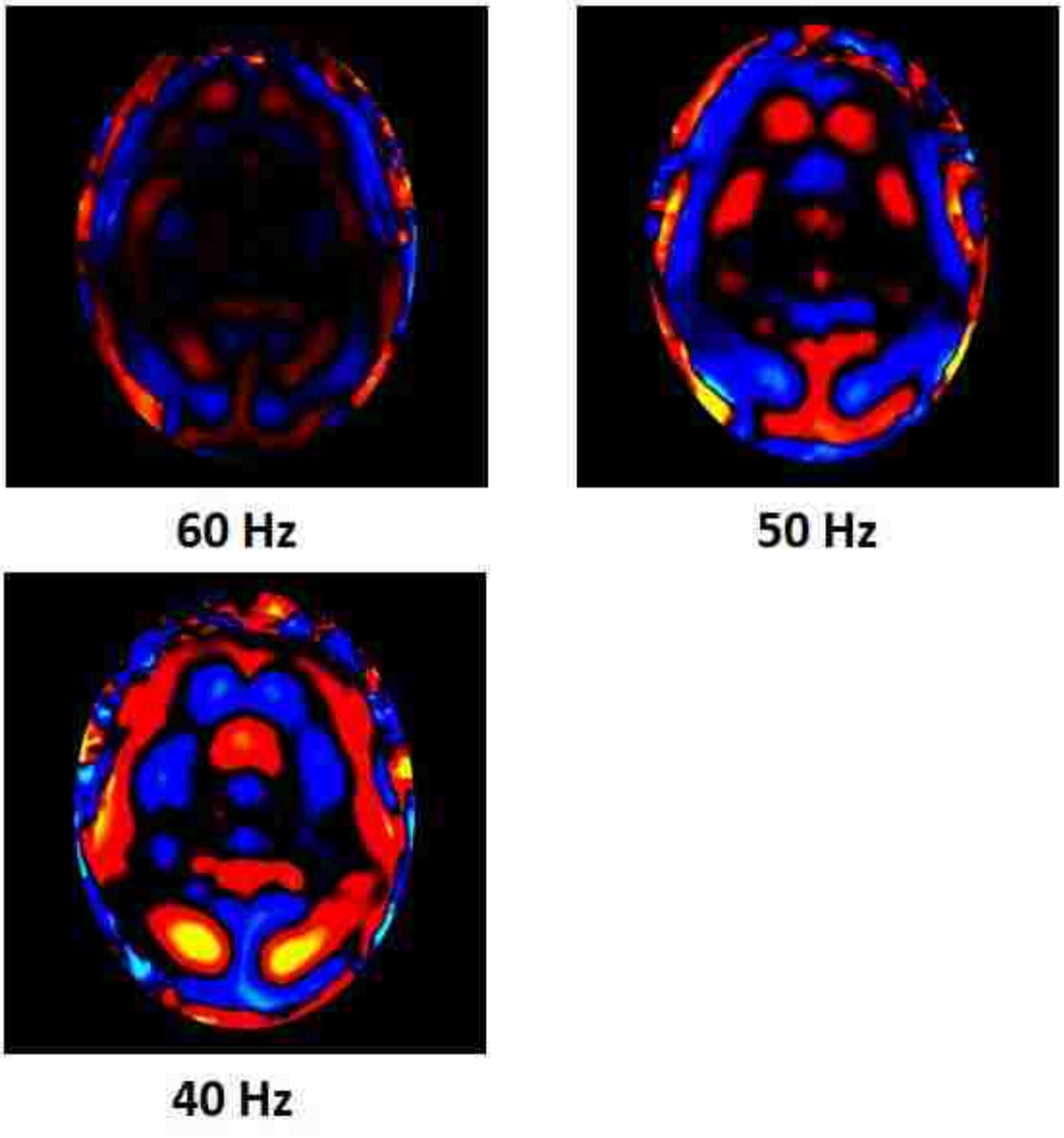

Figure A.6: Scan wave images for Subject 6 at 60 Hz (upper right), 50 Hz (upper left), and 40 Hz (bottom right).

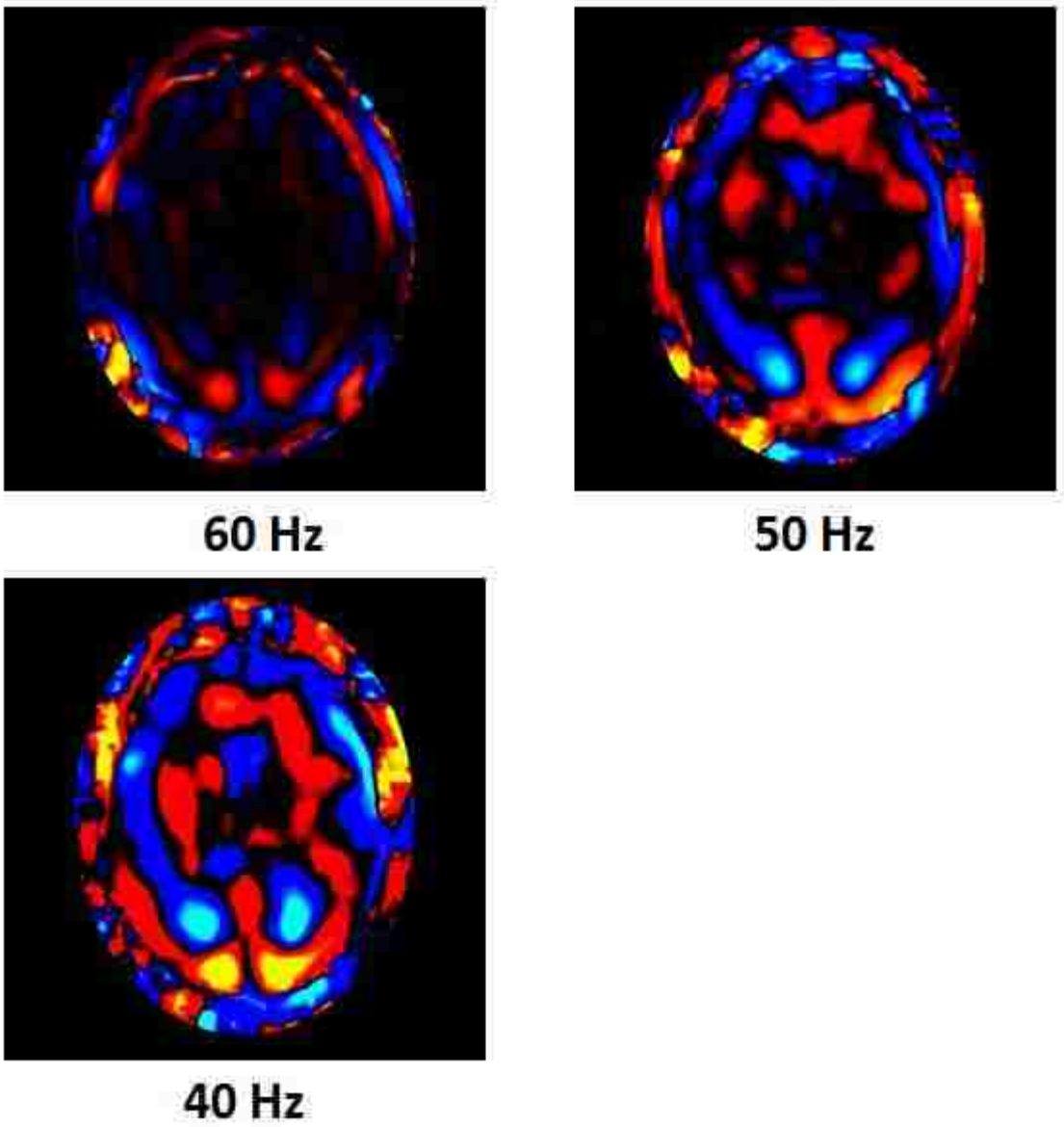

Figure A.7: Scan wave images for Subject 7 at 60 Hz (upper right), 50 Hz (upper left), and 40 Hz (bottom right).

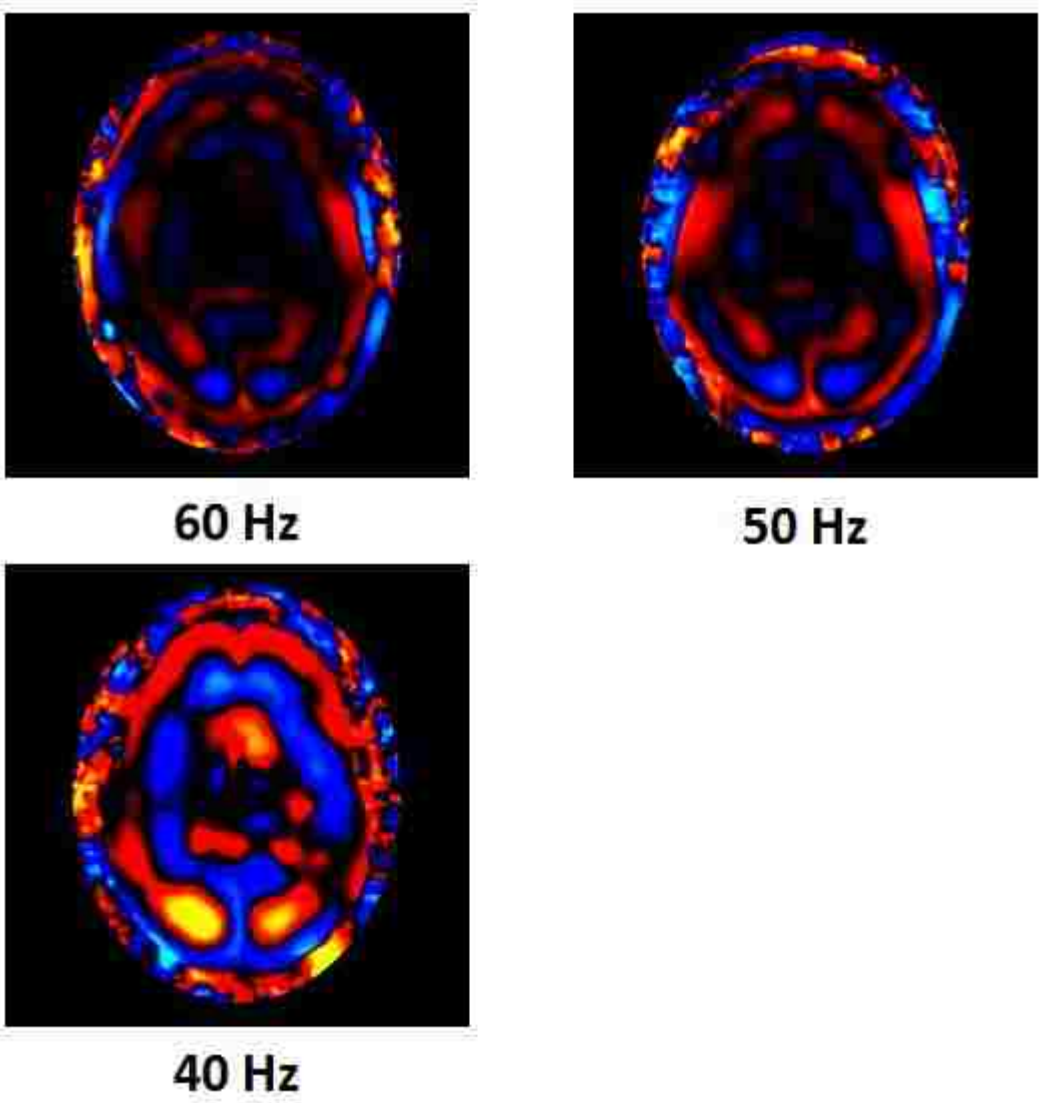

Figure A.8: Scan wave images for Subject 8 at 60 Hz (upper right), 50 Hz (upper left), and 40 Hz (bottom right).

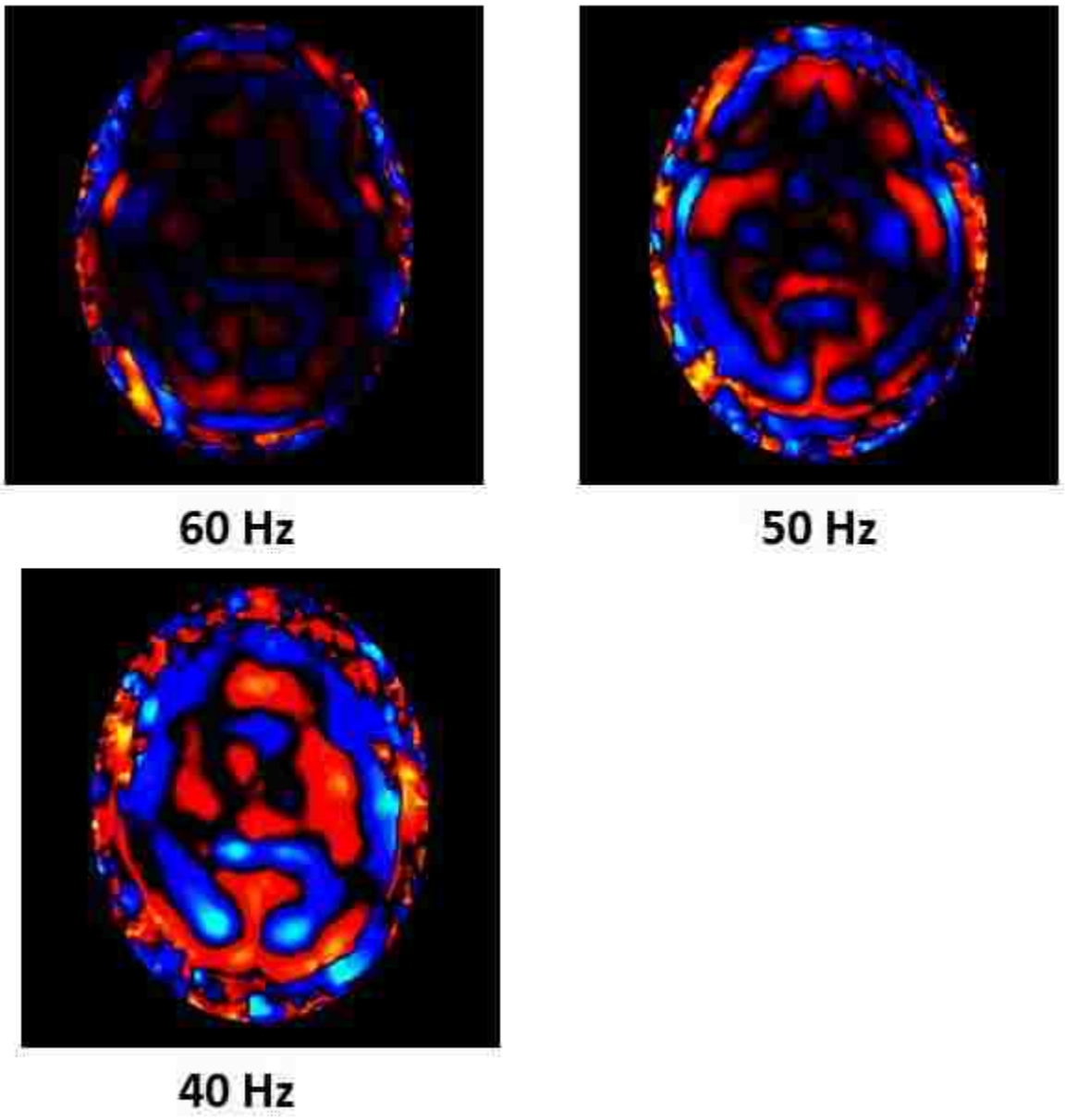

Figure A.9: Scan wave images for Subject 9 at 60 Hz (upper right), 50 Hz (upper left), and 40 Hz (bottom right).

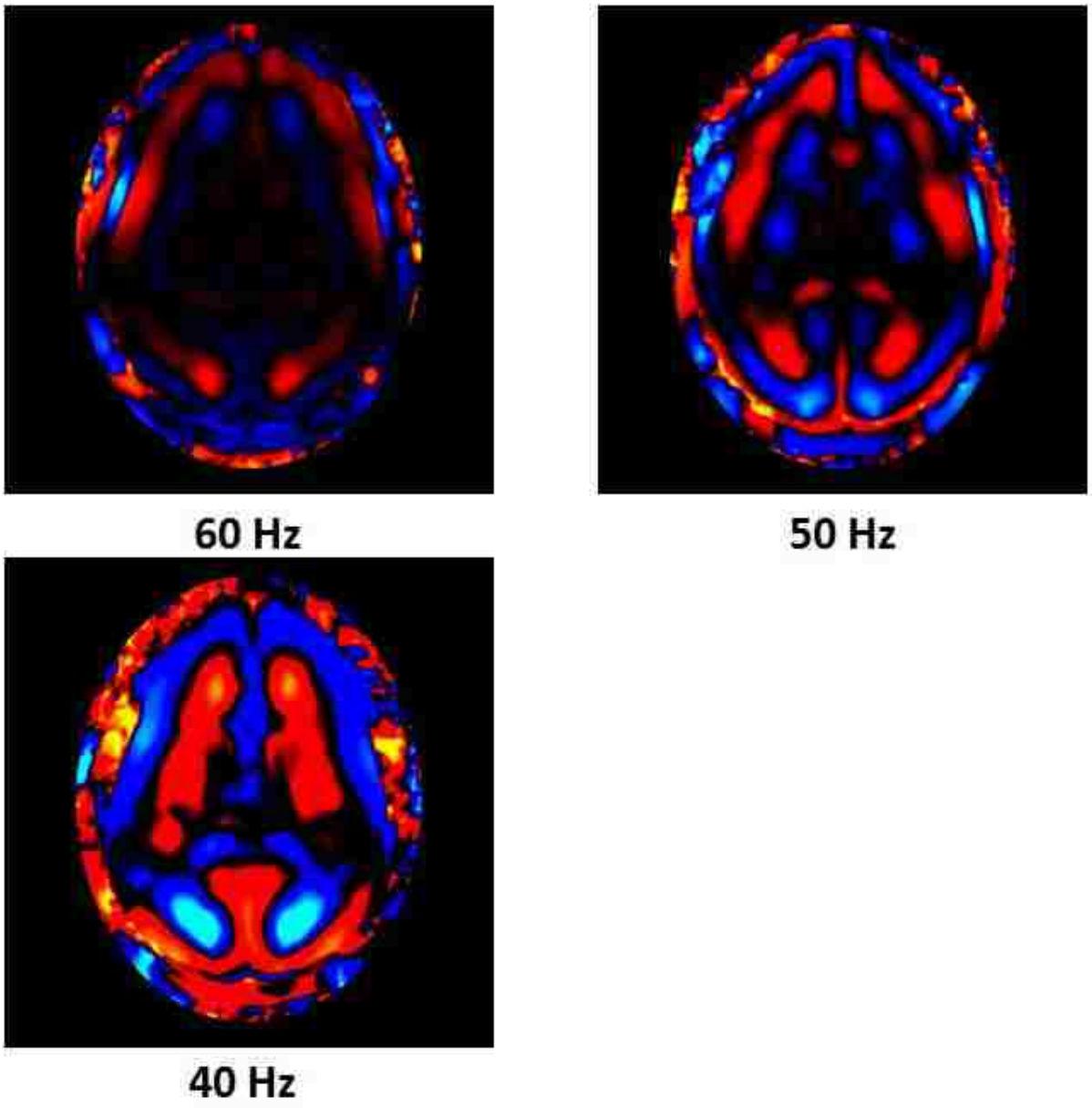

Figure A.10: Scan wave images for Subject 10 at 60 Hz (upper right), 50 Hz (upper left), and 40 Hz (bottom right).

APPENDIX B: ELASTOGRAM RESULTS FOR ALL SUBJECTS

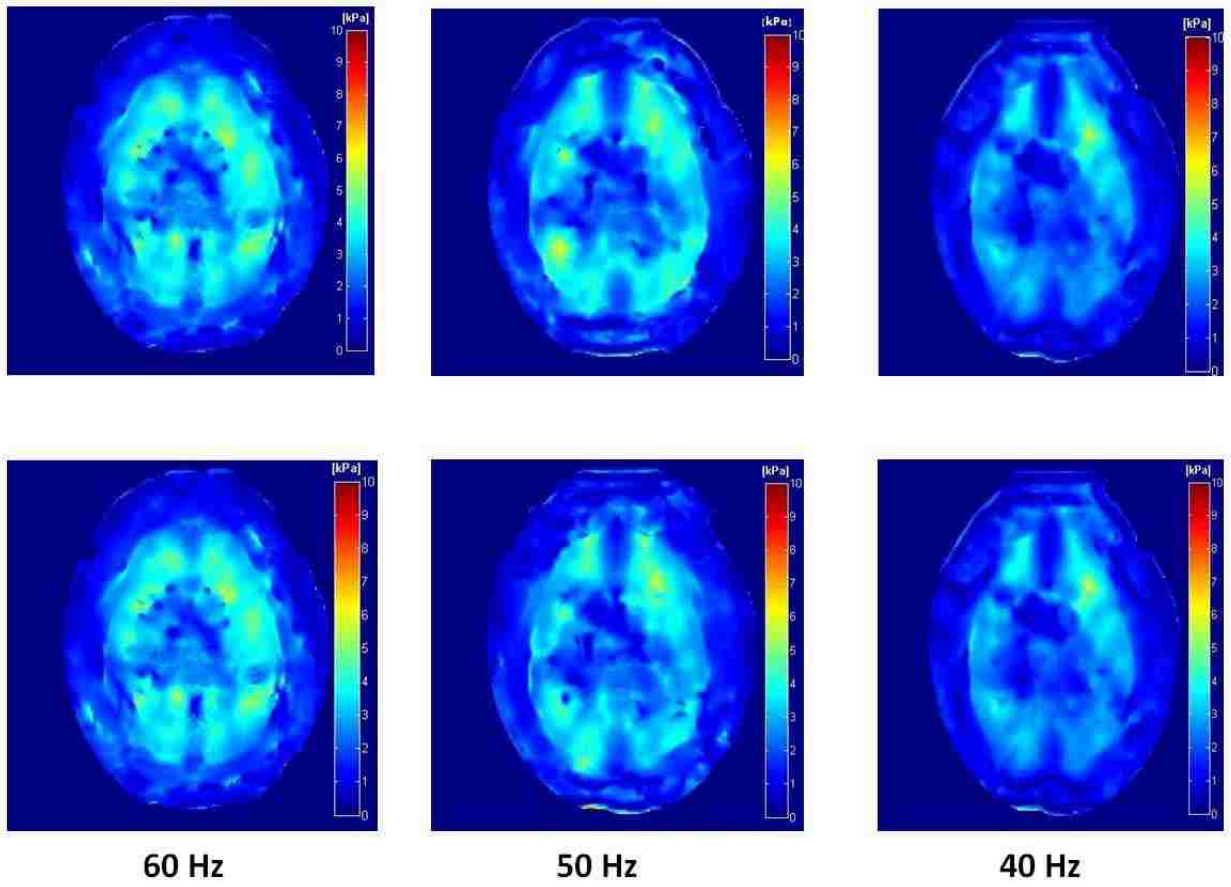

Figure B.1: Scan (upper row) and rescan (bottom row) elastograms for Subject 1 at 60 Hz (left), 50 Hz (middle), and 40 Hz (right).

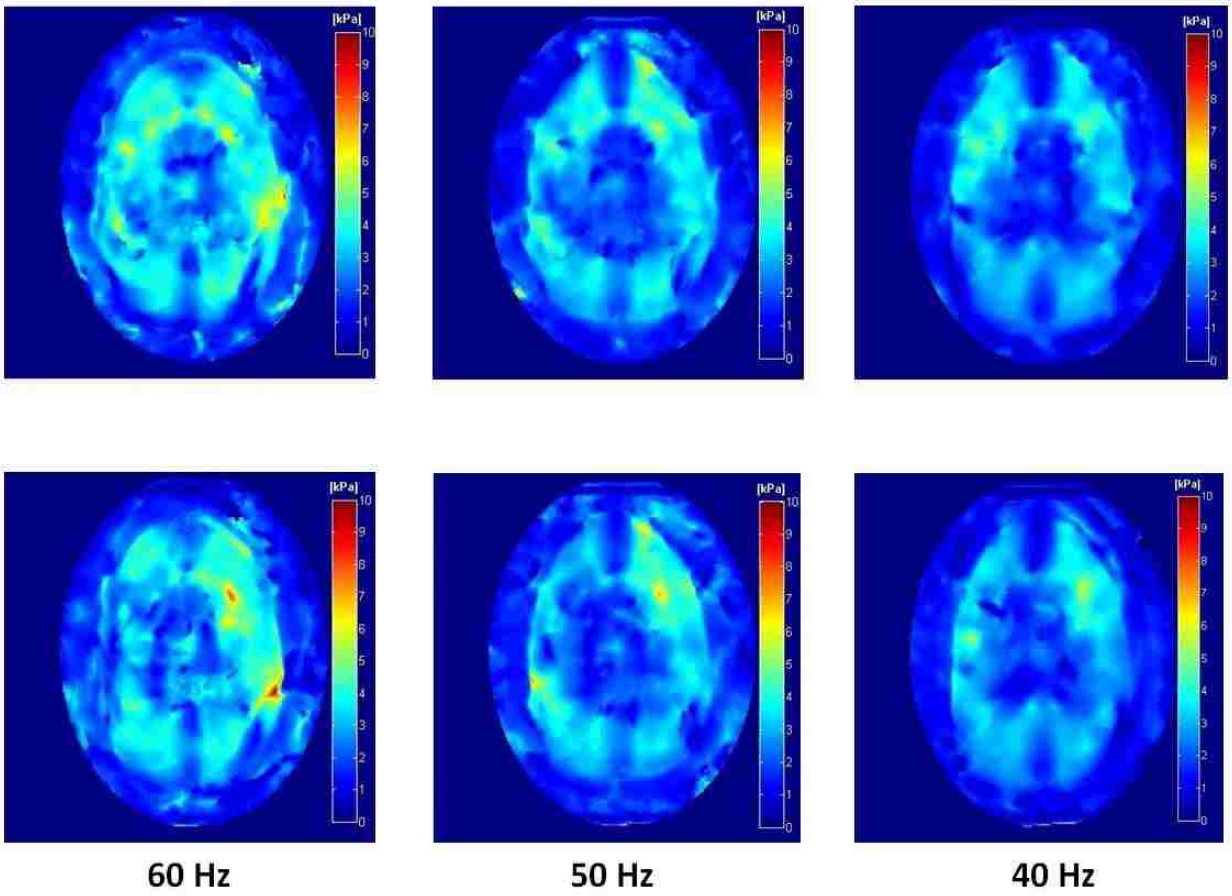

Figure B.2: Scan (upper row) and rescan (bottom row) elastograms for Subject 2 at 60 Hz (left), 50 Hz (middle), and 40 Hz (right).

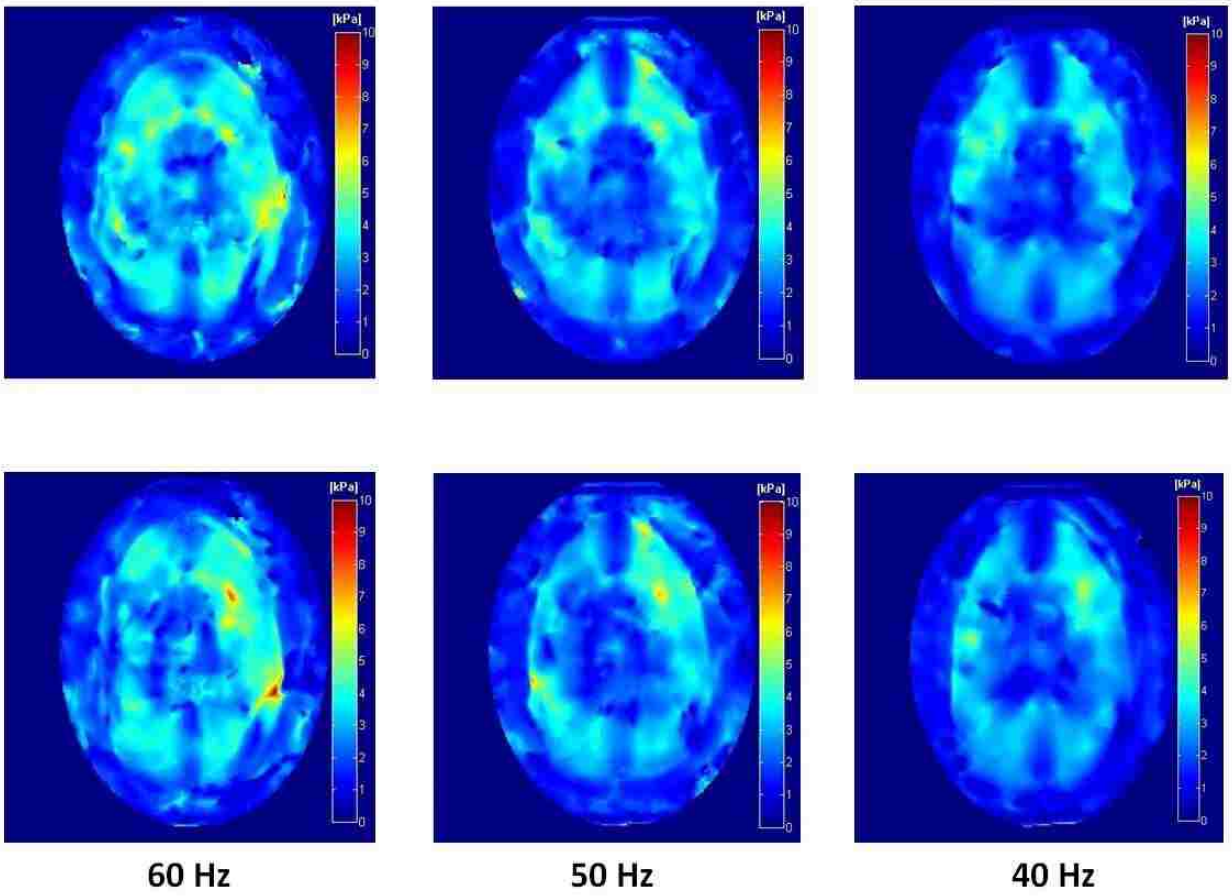

Figure B.3: Scan (upper row) and rescan (bottom row) elastograms for Subject 3 at 60 Hz (left), 50 Hz (middle), and 40 Hz (right).

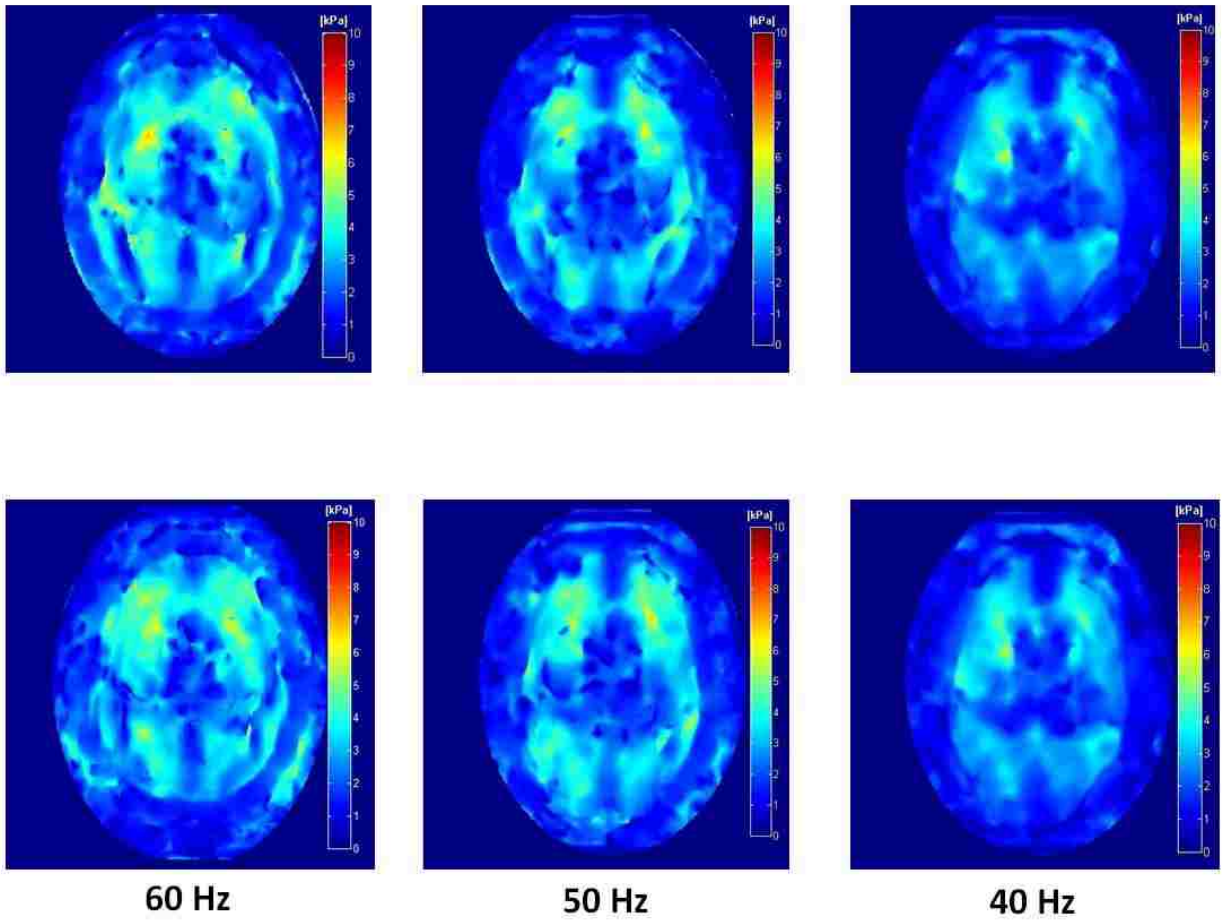

Figure B.4: Scan (upper row) and rescan (bottom row) elastograms for Subject 4 at 60 Hz (left), 50 Hz (middle), and 40 Hz (right).

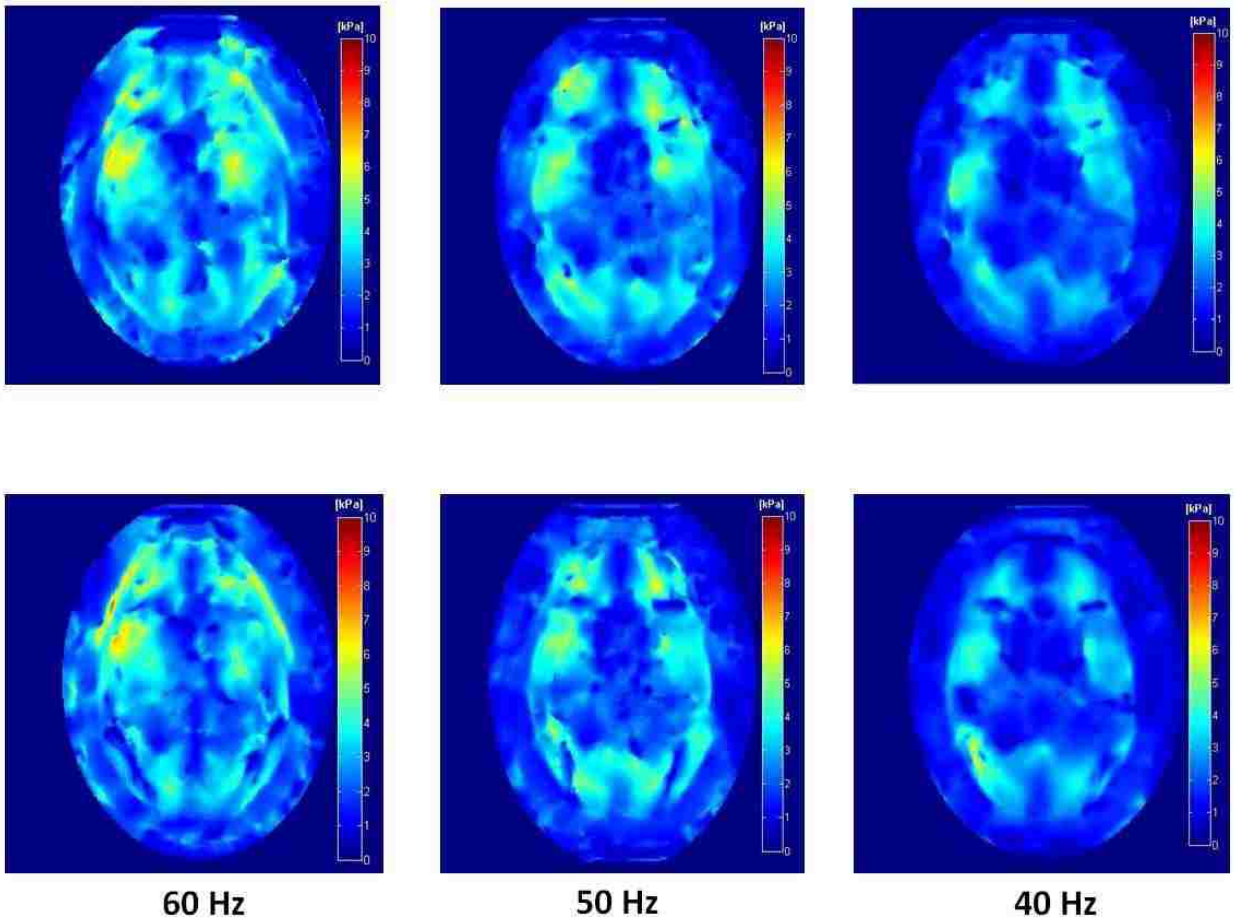

Figure B.5: Scan (upper row) and rescan (bottom row) elastograms for Subject 5 at 60 Hz (left), 50 Hz (middle), and 40 Hz (right).

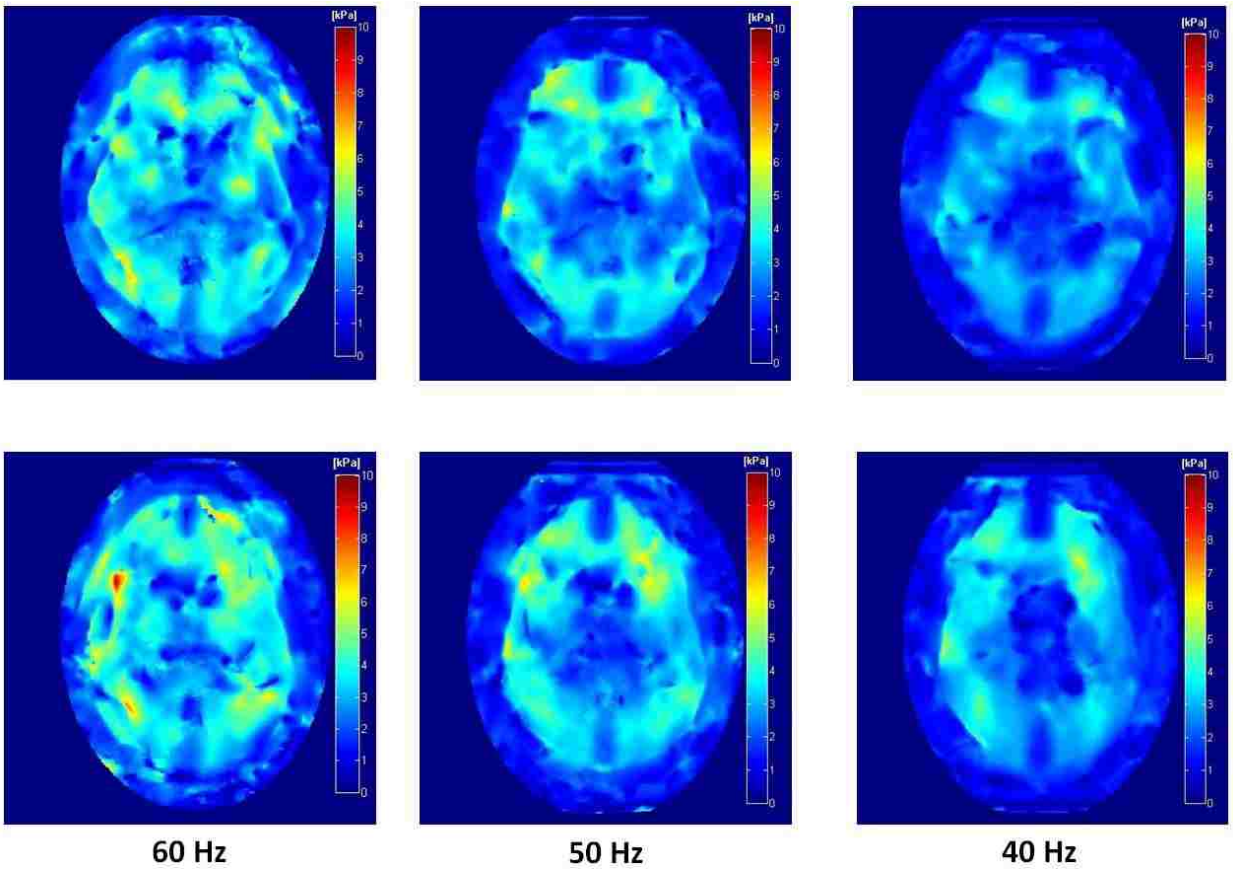

Figure B.6: Scan (upper row) and rescan (bottom row) elastograms for Subject 6 at 60 Hz (left), 50 Hz (middle), and 40 Hz (right).

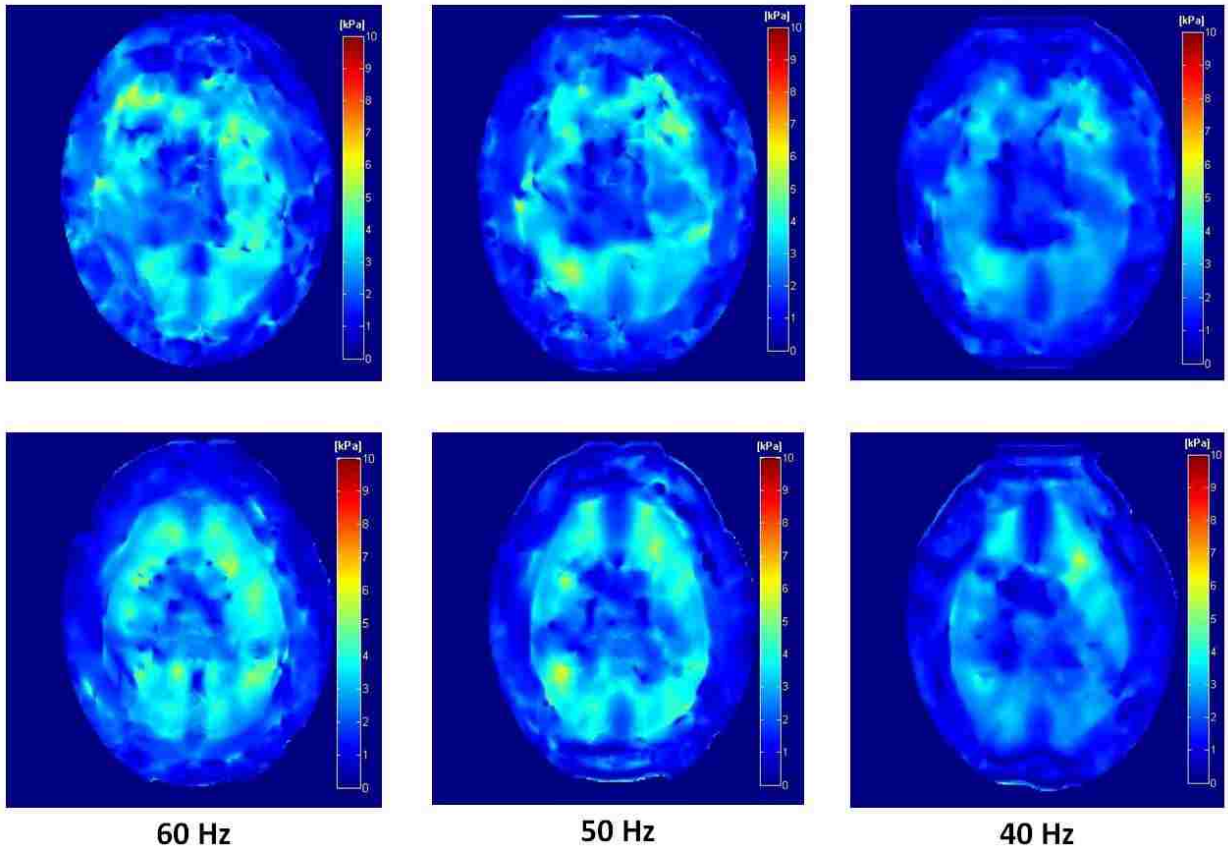

Figure B.7: Scan (upper row) and rescan (bottom row) elastograms for Subject 7 at 60 Hz (left), 50 Hz (middle), and 40 Hz (right).

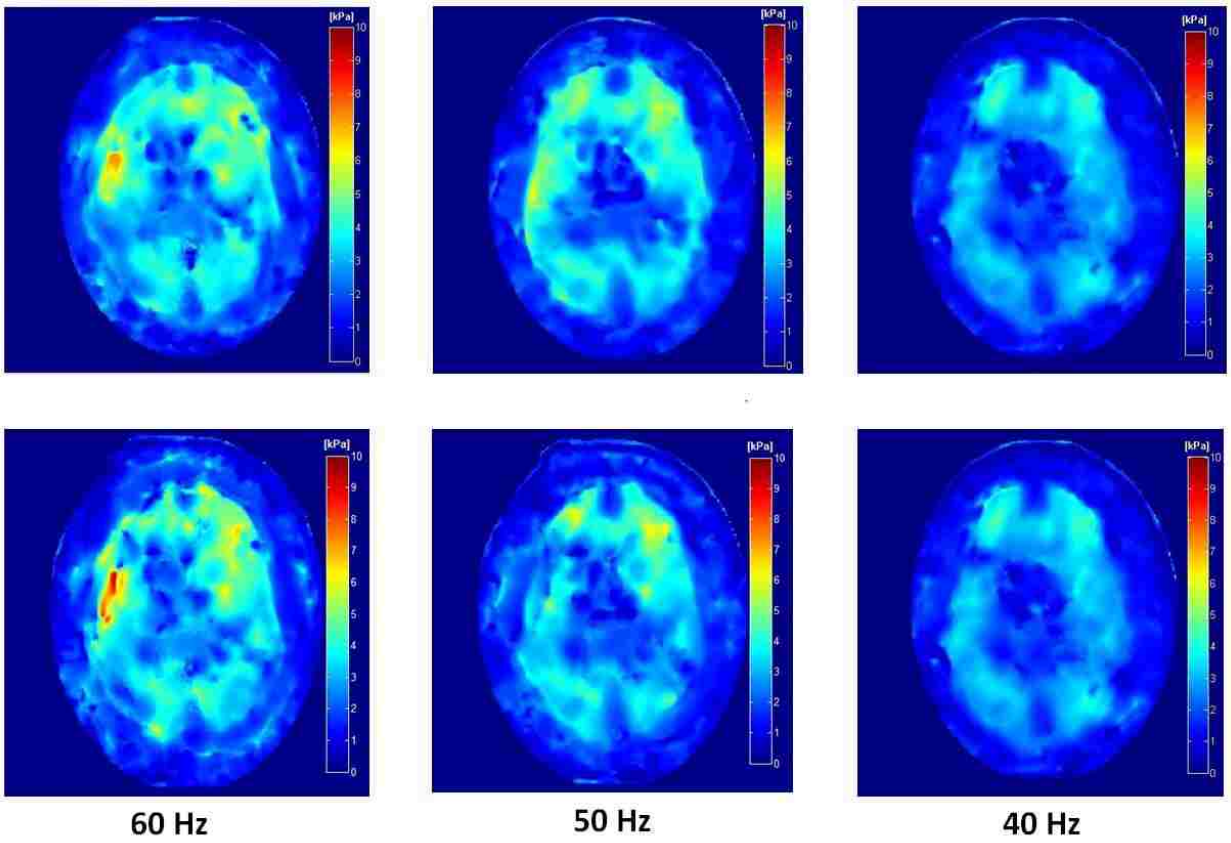

Figure B.8: Scan (upper row) and rescan (bottom row) elastograms for Subject 8 at 60 Hz (left), 50 Hz (middle), and 40 Hz (right).

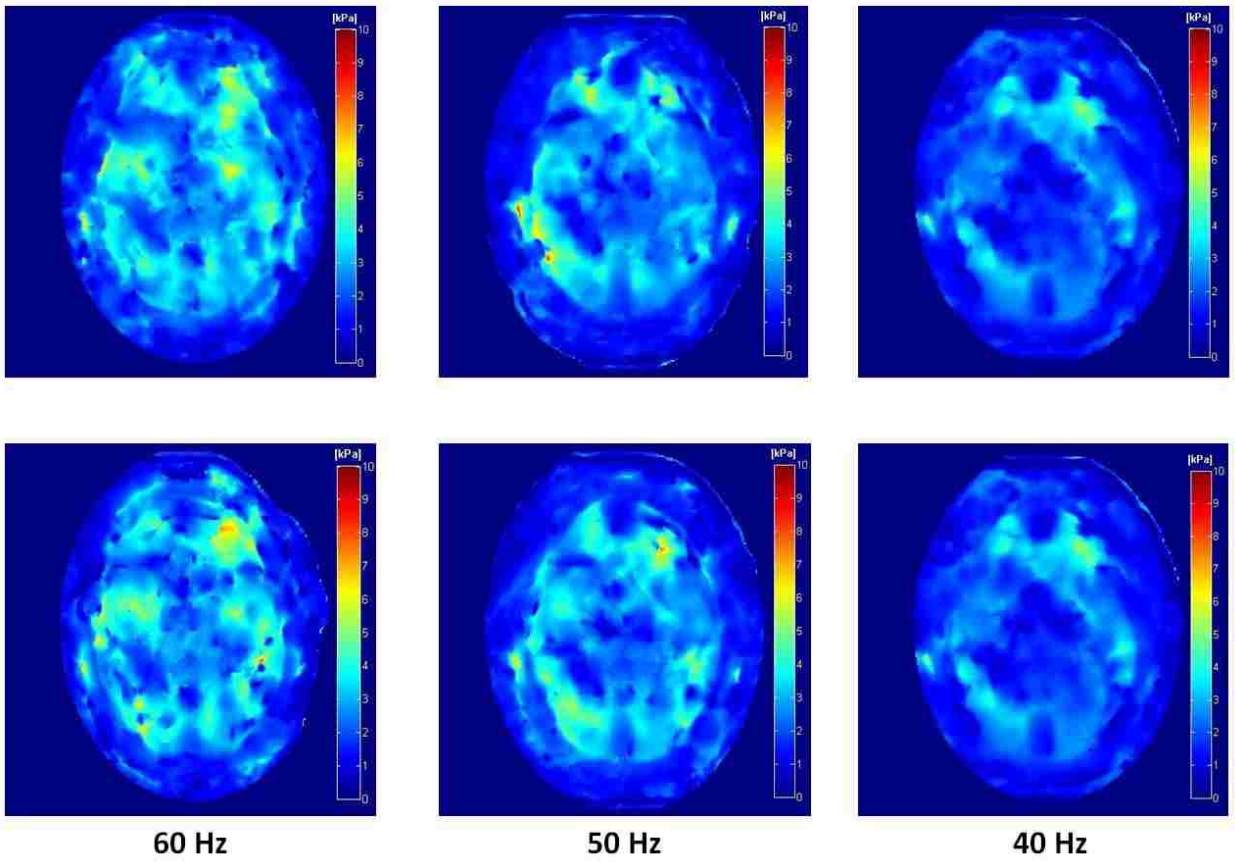

Figure B.9: Scan (upper row) and rescan (bottom row) elastograms for Subject 9 at 60 Hz (left), 50 Hz (middle), and 40 Hz (right).

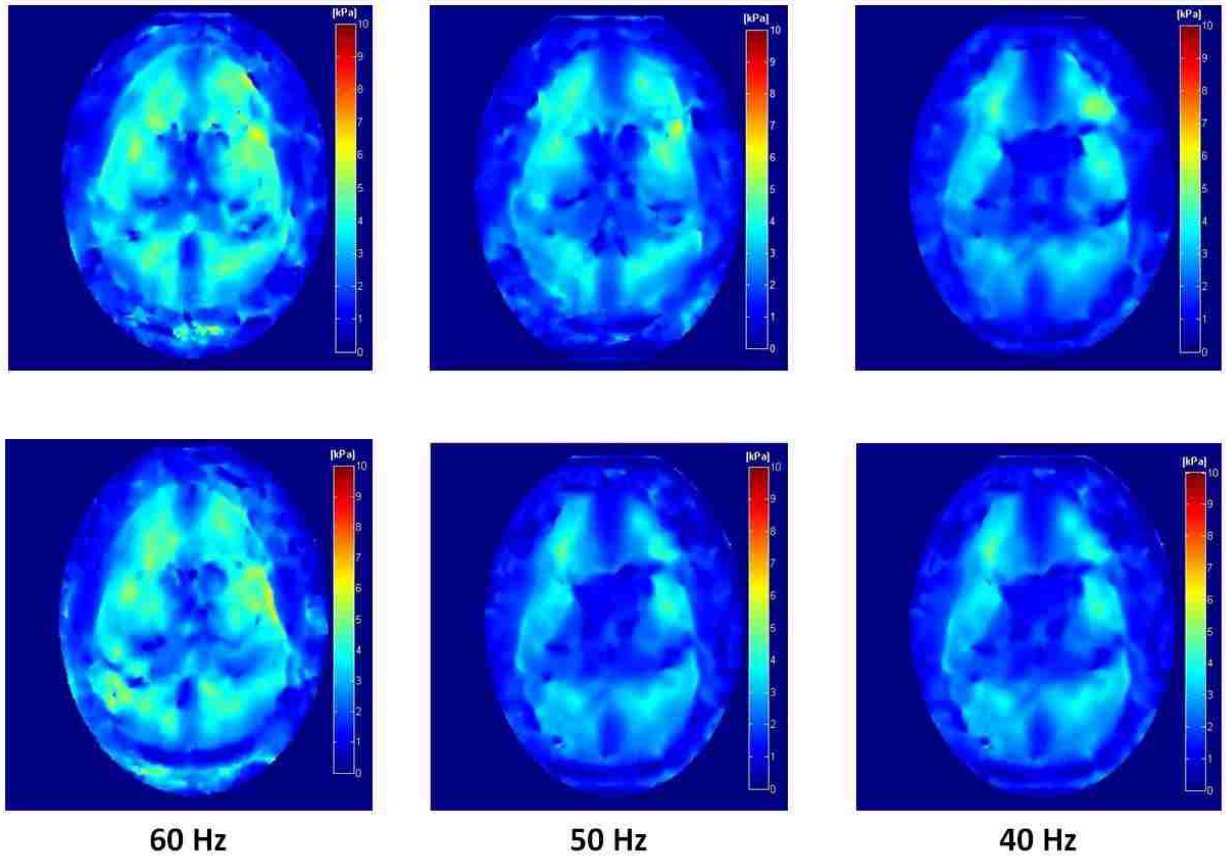

Figure B.10: Scan (upper row) and rescan (bottom row) elastograms for Subject 10 at 60 Hz (left), 50 Hz (middle), and 40 Hz (right).

VITA

Hatim Chafi was born in Casablanca, Morocco. He moved to Rockville, Maryland when he was thirteen years of age. He attended Richard Montgomery High School in Rockville, Maryland. Following high school graduation in summer 2003, he attended Duquesne University in Pittsburgh, Pennsylvania, receiving a Bachelor of Science degree in Business Administration in 2007. He also received a Bachelor of Science Degree in Physics from the University of Pittsburgh in 2012. In August of that same year, he enrolled in the Medical Physics Master's program at LSU. Following graduation from LSU he will begin medical physics residency training at Mary Bird Perkins Cancer Center in Baton Rouge, Louisiana.